Sensor Craft Control Using Drone Craft with Coulomb Propulsion System

Hyunsik Joe

Thesis submitted to the Faculty of the

Virginia Polytechnic Institute and State University

in partial fulfillment of the requirements for the degree of

Master of Science

in

Aerospace and Ocean Engineering

Hanspeter Schaub, Chair

Christopher D. Hall

Scott L. Hendricks

May 10, 2005

Blacksburg, Virginia

Keywords: Coulomb forces, Formation flying, Spacecraft, Sensor craft, Drone craft, Drone plane singularity

Sensor Craft Control Using Drone Craft with Coulomb Propulsion System

Hyunsik Joe

(ABSTRACT)

The Coulomb propulsion system has no exhaust plume impingement problem with neighboring spacecraft and does not contaminate their sensors because it requires essentially no propellant. It is suitable to close formation control on the order of dozens of meters. The Coulomb forces are internal forces of the formation and they influence all charged spacecraft at the same time. Highly nonlinear and strongly coupled equations of motion of Coulomb formation makes creating a Coulomb control method a challenging task. Instead of positioning all spacecraft, this study investigates having a sensor craft be sequentially controlled using dedicated drone craft. At least three drone craft are required to control a general sensor craft position in the inertial space. However, the singularity of a drone plane occurs when a sensor craft moves across the drone plane. A bang-bang control method with a singularity check can avoid this problem but may lose formation control as the relative distances grow bounded. A bang-coast-bang control method utilizing a reference trajectory profile and drone rest control is introduced to increase the control effectiveness. The spacecraft are assumed to be floating freely in inertial space, an approximation of environments found while underway to other solar system bodies. Numerical simulation results show the feasibility of sensor craft control using Coulomb forces.

Acknowledgments

I would like to thank my adviser, Dr. Hanspeter Schaub, for continuing to provide encouragement and mentoring in my academic career. This thesis would be impossible without his guidance toward my study. I am also grateful to my committee members, Dr. Christopher D. Hall and Dr. Scott L. Hendricks for their advices on this thesis. I am indebted to my family and my friends for their sincere support for me. Without their encouragement and optimism, I would not be able to complete my work.

Thanks again to all.

Contents

List of Symbols

a_{dec}	:	Constant sensor craft deceleration
d_{ij}	:	Relative distance between spacecraft i and j
d_p	:	Reference profile distance
$\boldsymbol{e}$	:	Distance error vector from the current position to the final position of sensor craft
e	:	The magnitude of $\boldsymbol{e}$
$\hat{e}$	:	The unit vector of $\boldsymbol{e}$
e_{aug}	:	Augmented position error of sensor craft
F_c	:	Coulomb force
$\boldsymbol{f}_c$	:	Sensor craft control force vector
$\hat{f}_c$	:	The unit vector of $\boldsymbol{f}_c$
$f_{c_{aug}}$	:	Augmented sensor craft control force
$\boldsymbol{f}_{ci}$	:	i^{th} drone craft control force vector
f_{dec}	:	Sensor craft deceleration force
f_{ij}	:	The Coulomb force of i^{th} spacecraft due to j^{th}

f_{si} : Coulomb force from i_{th} drone craft to sensor craft

$\boldsymbol{H}_d$: The summation of drone craft angular momentum vector about an inertial point

$\boldsymbol{H}_s$: The sensor craft angular momentum vector about an inertial point

$\boldsymbol{H}_t$: The total angular momentum vector of the system about an inertial point

$\boldsymbol{J}_s$: Matrix of $[\ \hat{r}_{s1} \quad \hat{r}_{s2} \quad \hat{r}_{s3}\ ]$

$\boldsymbol{J}_1$: Matrix of $[\ \hat{r}_{12} \quad \hat{r}_{13} \quad \hat{r}_{12} \times \hat{r}_{13}\ ]$

k_c : $8.99 \times 10^9 \mathrm{Nm}^2/\mathrm{C}^2$, The Coulomb's constant

k_d : The derivative gain of sensor craft control law

k_p : The proportional gain of sensor craft control law

m_i : i^{th} spacecraft mass

m_s : Sensor craft mass

q_i : i^{th} spacecraft charge

q_s : Sensor craft charge

$\boldsymbol{r}_i$: Inertial position vector of i^{th} spacecraft

$\hat{r}_{ij}$: Unit distance vector from j^{th} spacecraft to i^{th} spacecraft

$\boldsymbol{r}_f$: The final position vector of sensor craft

$\boldsymbol{r}_s$: The current position vector of sensor craft

$\hat{r}_{si}$: Relative distance unit vector from i_{th} drone craft to sensor craft

t_a : Sensor craft coast starting time

t_{d0} : Sensor craft deceleration starting time

v_p : Reference profile velocity

v_c : Sensor craft coasting velocity

$\boldsymbol{v}_i$: i^{th} spacecraft inertial velocity vector

$\boldsymbol{v}_{dpi}$: The projection velocity vector of i^{th} spacecraft on a drone plane

γ : Sensor craft deceleration band

λ_d : The Debye length

List of Figures

Chapter 1

Introduction

1.1 Motivation

Atmospheric image distortion issues can be avoided by placing observing sensors outside the Earth atmosphere. For instance, the Hubble space telescope transmits space images that contain more information than ever before[2]. A larger diameter of collector surface is required to improve the resolution and field of view of such an optic telescope or a radio telescope. However, there is a limitation on the size of monolithic satellite structures, because the fairing of a launch vehicle has a size restriction. Although one solution is the revision of the deployment system, the maximum diameter of the telescope is still limited and other structural problems may arise. Instead of a monolithic spacecraft system, several spacecraft can be organized to operate as one large space sensing system. The formation flying control

of spacecraft is required to realize such a space interferometry system.

For the acceptable performance of a space interferometry system, relative distances may need to be like as a few dozen meters. For the case of short relative distances of less than one hundred meters, conventional thruster systems for spacecraft formation control, such as gas jet thrusters or ion thrusters, have critical problems when the propulsion exhaust plume can impinge on neighboring spacecraft, and contaminate or damage their sensors. These problems are more serious as the relative distances decrease. It will require a great effort for close formation systems to be realized with conventional thrusters. To avoid these drawbacks, non-propellant thruster systems, such as tethered formation systems[6,18], electromagnetic systems[5,18], and electrostatic systems[3] have been studied. They have common advantages such as non-contamination of sensors of neighbor spacecraft and propellant-free thrusting for formation control. In this paper, an electrostatic method of propelling clusters of spacecraft, referred to as a Coulomb Spacecraft Formation (CSF), is considered. In particular, all spacecraft positions in the formation are not considered to be controlled at the same time, but sensor craft positions are controlled using drone craft. The drone craft act as electrostatic anchors, allowing the sensor craft to push and pull off them.

Coulomb forces are created between electrostatically charged objects. This charging method is clean and essentially propellant-free when compared to conventional thrusting technologies such as chemical or ion propulsion methods. Coulomb forces are based on the charge control of spacecraft, which has been studied and implemented for around twenty years. There is a recent research of spacecraft charging control[20]. In addition, Coulomb forces can be con-

tinuously generated using as little as 1 Watt of electrical power and have a high bandwidth. These advantages help to control a spacecraft formation or satellite cluster with high accuracy. Particularly, a Coulomb spacecraft formation is only applicable to high Earth orbit regions where the Debye length is much greater than the relative distance between spacecraft[8]. Contrarily, in low Earth orbit, the Debye length is on the order of centimeters and the electric fields are quickly absorbed by the local plasma environment. Thus, Coulomb forces are not effective to use to control close formations in low Earth orbit.

Internal Coulomb forces are used to maintain the formation and have no effect on the inertial angular momentum of the formation about the center of mass of the formation. The formation shape is adjusted using Coulomb forces without causing any inertial acceleration of the formation center of mass location. Parker et al.[12] proposed to separate sensor and drone spacecraft. The only purpose of the drone craft is to control the sensor craft position. The high control bandwidth of the Coulomb control enables this kind of control method. It is assumed that the drone craft have a conventional propulsion system to maneuver into a required position prior to controlling the sensor craft. Such a propulsion system is inactive while the Coulomb propulsion system is used to reposition sensor craft. They considered the case where three drone craft were used to control a single sensor craft to move it to any desired position. However, there is a limitation of this control strategy when a sensor craft moves across the drone plane formed by the three drone craft. If a sensor craft is initially located at rest out of the drone plane and a desired position is located on the same side, the reposition control works. In contrast, if a sensor craft is initially located on a drone

plane and a desired position is located either side of a drone plane, then it is impossible to reposition a sensor craft with a Coulomb propulsion system. This situation is referred to as a singularity of a drone plane. This singularity is caused by the fact that Coulomb forces are internal forces of the formation. If all craft are located on the same plane, there is no force out of the plane. Therefore, this thesis contains research of sensor craft Coulomb control while considering this singularity. First, a bang-bang control method is studied with the singularity. Numerical simulations show the performance of the bang-bang control and other implementation problems. To solve the problem, a revision of the bang-bang control is presented and numerical simulations show the performance difference between two control methods.

1.2 Coulomb Propulsion Background

In higher Earth orbit, there is a hot plasma caused by the interaction between Earth's magnetic field and the solar wind. When a spacecraft is located in this plasma field, the spacecraft can naturally be charged with high negative voltages[9]. If there are at least two charged spacecraft, and we can adjust charge levels of each spacecraft with charge control equipment, the interaction force can be controlled so that the spacecraft push or pull off each other. This interaction force is called Coulomb force, is caused by two or more charged bodies, and follows Coulomb's law as

$$F_c = k_c \frac{q_i q_j}{d_{ij}^2} e^{-\frac{d_{ij}}{\lambda_d}} \qquad (i \neq j) \tag{1.1}$$

where F_c is the Coulomb force magnitude, k_c is 8.99×10^9 Nm^2/C^2 Coulomb's constant, q_i is the charge of i^{th} spacecraft, d_{ij} is the relative distance between spacecraft i and j, and λ_d is the Debye length. As can be seen in Figure 1.1, Coulomb forces act along the line connecting two charges, and the direction of the Coulomb force depends on the sign of the charges.

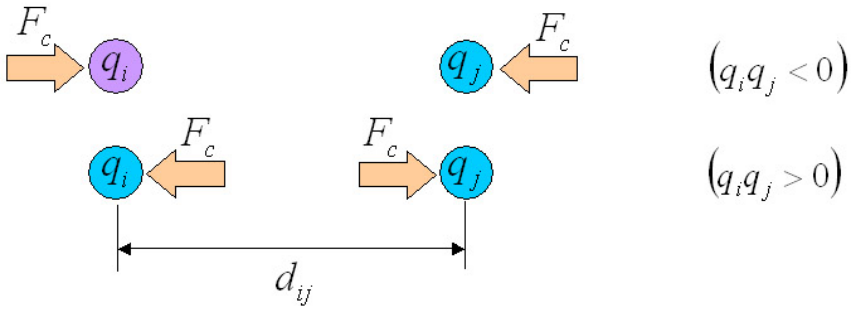

Figure 1.1: Coulomb forces

To utilize the Coulomb force in a space environment, the relative distances should be smaller than the Debye length. In high Earth orbit (HEO), this length can be greater than one thousand meters, while only dozens of centimeters in low Earth orbit (LEO). Coulomb force is a significant force in HEO for relative motion control when compared to other perturbation forces[13].

If there are spacecraft in inertial space without any external force, the equations of motion of charged spacecraft are simply given by

$$\ddot{\boldsymbol{r}}_i = \frac{k_c}{m_i} \sum_{j=1}^{n} \frac{\boldsymbol{r}_i - \boldsymbol{r}_j}{\|\boldsymbol{r}_i - \boldsymbol{r}_j\|^3} q_i q_j \qquad (i \neq j) \tag{1.2}$$

where $\boldsymbol{r}_i$ is the inertial position vector of spacecraft i, and m_i is the mass of spacecraft i.

This equation is valid in the region of the large Debye length and gravitational cancellation such as the Lagrange points. In HEO, the exponential part of Eq. (1.1) is approximately unity when the relative distance is much smaller than the Debye length.

1.3 Literature Review

In 1979, the SCATHA (Spacecraft Charging at High Altitude) satellite was launched to collect plasma field data in HEO and to test spacecraft charging[10]. An electron gun and a positive ion gun were installed in the SCATHA satellite to control the level of the spacecraft potential. The experiment results showed the possibility of generating control forces to accelerate or decelerate a spacecraft.

There has been other flight experiments where spacecraft charging control was used. The Geotail and Equator-S spacecraft were launched in 1992 and 1997 respectively[19]. Ion emitters with liquid metal ion sources were used to control spacecraft charge. The emitter module installed on the Geotail operated over six years without any flaw and the instrument in the Equator-S worked 4000 hours successfully. Torkar et al.[20] showed the results of the experiment with charging control of the Cluster spacecraft using emitters of the liquid metal ion source type described in Reference[19].

King et al. in References[3,4,8] studied formation control with Coulomb forces in higher Earth orbit. They paid attention to the close formation without payload contamination which is due to current micropropulsion systems such as micro-pulsed-plasma thrusters, field-emission

electric propulsion thrusters, and colloid thrusters. They proposed using Coulomb forces between the spacecraft for close formation control. The Coulomb propulsion is essentially clean and propellantless. Thus, the sensor contamination problem can be avoided and the spacecraft life can be extended. Chong[3] analyzed the stability and controllability of various Coulomb formations using the linearization of Hill's equation. Deshmukh[4] investigated the implementation and the distinguished advantages of Coulomb formation control comparing to the propellant exhaust systems. To avoid contaminating sensors of neighboring spacecraft, tethered formation system[6,18] or electromagnetic system[5,18] can be a solution.

Schaub et al.[13] researched the static equilibrium conditions of Coulomb spacecraft formations as well as nonlinear bounding control laws of two satellites of Coulomb formation in a geosynchronous orbit. Berryman et al.[1] searched for equilibrium configurations of Coulomb formations using an evolutionary algorithm. Spacecraft dynamics were expressed in the Hill frame. They found static equilibria but did not show it they are stable or controllable. Natarajan et al.[11] used Coulomb force as a virtual tether to stabilize a two-satellite nadir formation. A Coulomb force was used to control relative distance between the two satellites, while the attitude was stabilized by the gravity gradient torque. Joe et al.[7] researched the barycenter of Coulomb formation and introduced fluid-like formation body frame to study formation shape and attitude changes and control them. Schaub et al.[16] investigated the formation center-of-mass and the conservation of the angular momentum of the formation using orbit element differences with first order constraints of Coulomb formation. Schaub[15] studied stabilizing charging control law with consideration of more than two spacecraft with

unequal masses and individual charging limits using an orbit element difference formulation. Parker et al.[12] investigated sensor craft control using drone craft to avoid the complexity of highly coupled nonlinearity of Coulomb formation. They excluded the singularity of drone plane which may occur during a sensor craft moves. In this thesis, the singularity avoidance method will be studied to expand the sensor craft movement.

1.4 Overview of thesis

This thesis consists of four chapters. Chapter 1 contains the motivation of this research, the background of the Coulomb propulsion concept, and the literature review of the spacecraft charging control and the Coulomb spacecraft formation. Chapter 2 describes the sequential method of the sensor craft reposition control and the drone craft rest control. How to avoid drone plane singularity is explained and numerical simulation shows the advantage and disadvantage of the bang-bang control method. The bang-coast-bang control method that reduces the failure possibility of the bang-bang control method is investigated in Chapter 3. Reference profile effect and angular momentum study are shown with numerical simulation. The bang-coast-bang control results are compared with the bang-bang control results. The thesis concludes with Chapter 4, which summarizes the achievement of this research, discusses the limitation of the results and the further studies of Coulomb spacecraft formation.

Chapter 2

Bang-Bang Control

The control strategy is to move sensor craft to their final positions using drone craft using only Coulomb propulsion. The control scheme is composed of two parts: Step 1) the reconfiguration of sensor craft, and Step 2) stopping all drone spacecraft motion after the sensor has been placed at the target[12]. To simplify the problem, three drone craft are used to control a single sensor craft and there is no external force in the inertial reference frame. Although spacecraft fly under various space environments; gravity gradient field, magnetic field, orbit rate, and so on, such effects are excluded to focus on the feasibility of using a Coulomb control force to position a sensor craft in this elementary level study. All spacecraft are assumed to be at rest before the sensor craft maneuver begins and after achieving the control objective.

Figure 2.1 shows the configuration of the problem. The shadowed triangle is a drone plane

which is defined by the positions of the drone craft. The large solid arrows indicate that maximum control forces that are acting on the sensor craft. The maximum control force magnitude changes because a control force is determined by the relative distances and charges. Though the relative distance changes, the charge of the sensor spacecraft can be fixed at its maximum. Thus, the control force magnitude can be maximum even though a sensor craft moves.

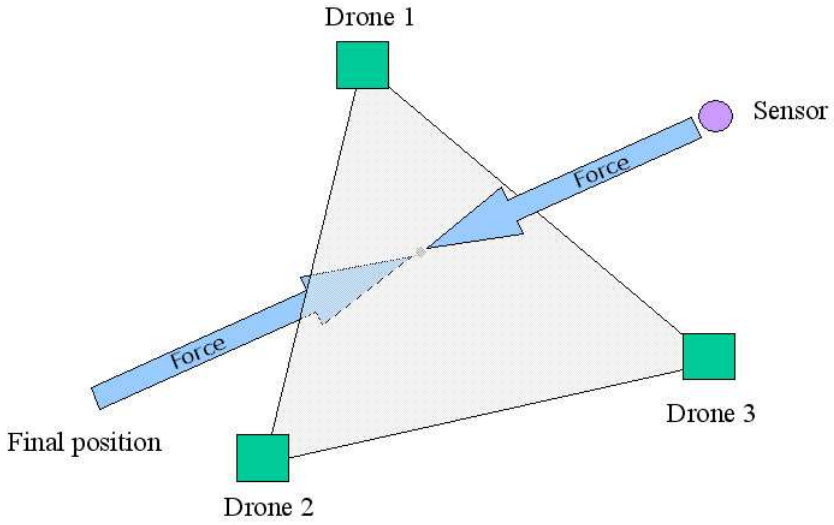

Figure 2.1: Bang-bang control

The first control step is that all drone craft are used to reposition a sensor craft. In this stage, the positions and velocities of the drone craft are not control parameters. However, the relative distances between drone craft are considered to avoid collision. After the sensor craft completely stops at the final position, the second step begins. Here we attempt to stop one of the drone craft at an arbitrary position using the Coulomb forces due to the other two drone craft. The final step is that the two remaining drone craft help each other to stop

in the inertial frame. The sequence control of Parker et al.[12] is summarized in the following two sections.

2.1 Step 1: Sensor Craft Position Control

Coulomb forces are formation internal forces. The Coulomb force between two spacecraft always lies on the line connecting them. Therefore, the net force on the sensor craft is the summation of the Coulomb forces between the sensor craft and other drone craft and this force is easily computed by vector addition. As can be seen from Figure 2.2, this net force is considered as the control force ($\boldsymbol{f}_c$) to adjust the sensor craft position and velocity. All vectors are expressed in the inertial reference frame of X, Y, and Z.

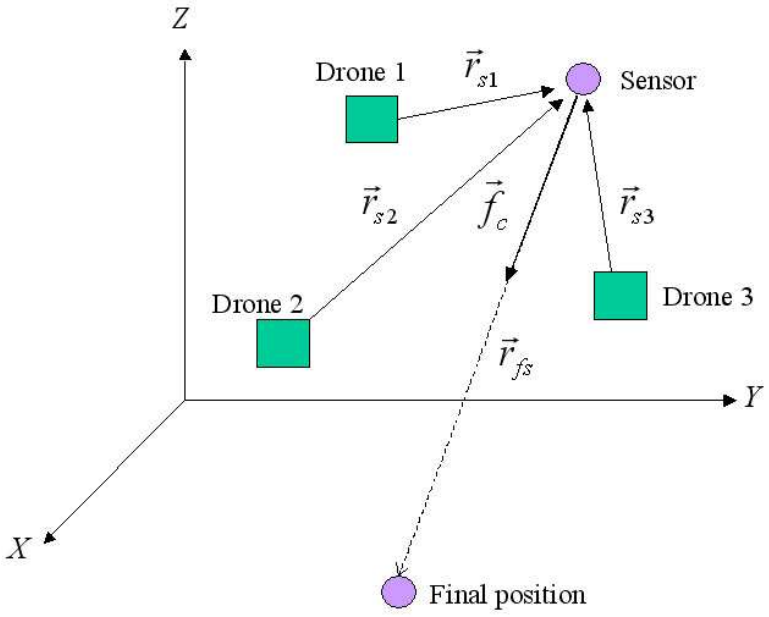

Figure 2.2: Configuration of sensor and drone craft

The control force of a sensor craft is described by

$$\boldsymbol{f}_c = f_{s1}\hat{r}_{s1} + f_{s2}\hat{r}_{s2} + f_{s3}\hat{r}_{s3} \tag{2.1}$$

where f_{si} is the force acting on the sensor craft from the i^{th} drone craft and $\hat{r}_{si}$ is the unit vector from the i^{th} drone craft to the sensor craft. Because there are three drone craft to control the sensor craft, the individual relative Coulomb forces can be calculated using the matrix inverse of relative distance unit vectors and designed control force through

$$\begin{bmatrix} f_{s1} & f_{s2} & f_{s3} \end{bmatrix}^T = \boldsymbol{J}_s^{-1}\boldsymbol{f}_c \tag{2.2}$$

where

$$\boldsymbol{J}_s = \begin{bmatrix} \hat{r}_{s1} & \hat{r}_{s2} & \hat{r}_{s3} \end{bmatrix} \tag{2.3}$$

The charge of the sensor craft has two values, maximum charge value and zero. When the control of the sensor craft is active, then the sensor craft has the maximum charge. After a sensor craft comes to rest, its charge is set to zero to maintain the final position. Therefore, the charge of a drone craft is determined by the constant charge of the sensor craft to generate each required force, f_{si}. The charge of each drone craft is computed using

$$q_i = \frac{f_{si}\|\boldsymbol{r}_{si}\|^2}{q_s k_c} \qquad (i = 1, 2, 3) \tag{2.4}$$

Total control force, f_c, is produced by a stabilizing control law. Parker et al.[12] proposed a simple PD control law acting on the sensor craft to the final position. The control force only acts on the line of sight from the initial sensor craft position to the final position until the

sensor craft arrives at the final position. The position and velocity errors are defined by this fact and are expressed as

$$\boldsymbol{e} = \boldsymbol{r}_f - \boldsymbol{r}_s \tag{2.5}$$

$$e = \boldsymbol{e} \cdot \hat{e} \tag{2.6}$$

$$\dot{e} = -\dot{\boldsymbol{r}}_s \cdot \hat{e} \tag{2.7}$$

where $\boldsymbol{r}_f$ is the final position vector, $\boldsymbol{r}_s$ is the present position vector of a sensor craft, and $\hat{e}$ is the unit vector of error.

Because the direction of the error vector is the same as that of the total control force vector, the unit vector of the total control force is described by

$$\hat{f}_c = \hat{e} \tag{2.8}$$

Finally, the magnitude of the total control force vector is computed by

$$f_c = k_p e + k_d \dot{e} \tag{2.9}$$

where k_p is a proportional gain, k_d is a derivative gain.

The charge of a drone craft is proportional to the control force. If the total control force is large, then the interacting force between the sensor craft and each drone craft should be large. Large charge of a drone craft causes a large relative force between drone craft. This fact means that the magnitude of the relative velocity between the drone craft will increase. Thus, drone craft can repel from each other with a high speed, which causes a loss of the

sensor craft position control, or some of the drone craft can attract each other with a high speed and collision may occur if there is no collision avoidance process.

There is a simple method to restrain increasing relative velocity of the drone craft. If the constant charge of the sensor craft is bigger than the maximum charge of a drone craft, and the mass of the sensor craft is smaller than that of a drone craft, then the required charge of each drone craft will be smaller than when the maximum charges of sensor and drone craft are the same. Therefore, relative forces between drone craft are smaller and hence the relative accelerations are smaller. This effect is discussed further in Section 2.5.

2.2 Step 2: Drone Craft Rest Control

It is assumed that all spacecraft are at rest before the sensor craft starts to move and the total momentum of the spacecraft formation is zero. After a sensor craft stops at its final position, all drone craft are moving in the drone plane, whose orientation and position are fixed in inertial space. Figure 2.3 shows that the sensor craft is at rest and the velocity vectors of the drone craft lie in the drone plane.

Drone rest control is similar to the control explained in Section 2.1 except that there is no specific position control. Rather, the goal of Step 2 is to control all drone craft positions at arbitrary positions. One drone craft's motion can be stopped by the other two drone craft. Since relative forces lie on the plane, and there is no out-of-plane force, no drone craft can escape from the drone plane. Therefore, the control force acting on the first drone craft to

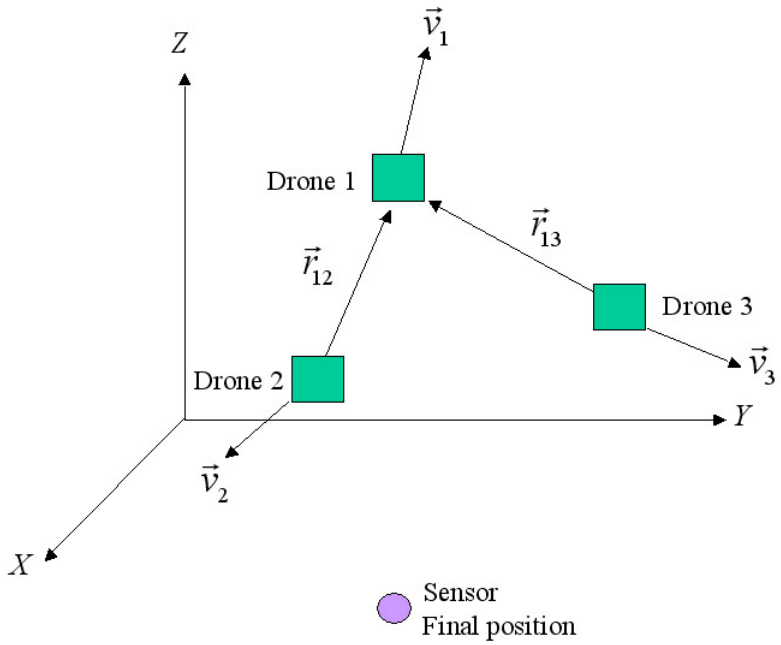

Figure 2.3: Drone rest control

stop this craft is described as

$$\boldsymbol{f}_{c1} = f_{12}\hat{r}_{12} + f_{13}\hat{r}_{13} \tag{2.10}$$

where f_{12} and f_{13} are relative forces between first drone craft and others, and $\hat{r}_{12}$ and $\hat{r}_{13}$ are relative distance unit vectors. Equation (2.10) is a vector equation and two forces need to be determined. Since there is no out-of-plane force acting on the first drone craft, the relative forces are calculated by

$$\begin{bmatrix} f_{12} & f_{13} & 0 \end{bmatrix}^T = \boldsymbol{J}_1^{-1}\boldsymbol{f}_{c1} \tag{2.11}$$

where

$$\boldsymbol{J}_1 = \begin{bmatrix} \hat{r}_{12} & \hat{r}_{13} & \hat{r}_{12} \times \hat{r}_{13} \end{bmatrix} \tag{2.12}$$

The charge of the first drone craft is constant and the charges of the other two craft are determined by

$$q_i = \frac{f_{1i}\|\boldsymbol{r}_{1i}\|^2}{q_1 k_c} \quad (i = 2, 3) \tag{2.13}$$

The objective of the drone rest control strategy is to make the velocity of all drone craft go to zero. The desired control force has the same direction as the velocity vector of the first drone craft and the magnitude of the force is determined by a control gain and the velocity :

$$\hat{f}_{c1} = \hat{v}_1 \tag{2.14}$$

$$f_{c1} = -k_d v_1 \tag{2.15}$$

After the first drone craft is at rest, the other two drone craft are still moving. The motion is restricted to the line that connects the two craft. This fact means that the second and third drone craft move along the line and the required control force lies on the line. As can be seen from Figure 2.4, the first drone craft and the sensor craft are at rest and the second and the third drone craft still move along a line. The relative distance vector, $\boldsymbol{r}_{23}$, has the same direction and only the length of the vector changes.

Thus, this linear motion of the second drone craft is described as

$$m_2 \ddot{r}_{23} = f_{c2} = 2f_{23} \tag{2.16}$$

$$f_{c2} = \frac{2k_c q_2 q_3}{r_{23}^2} \tag{2.17}$$

In this stage, the charge of the second drone craft is constant and the required charge of the

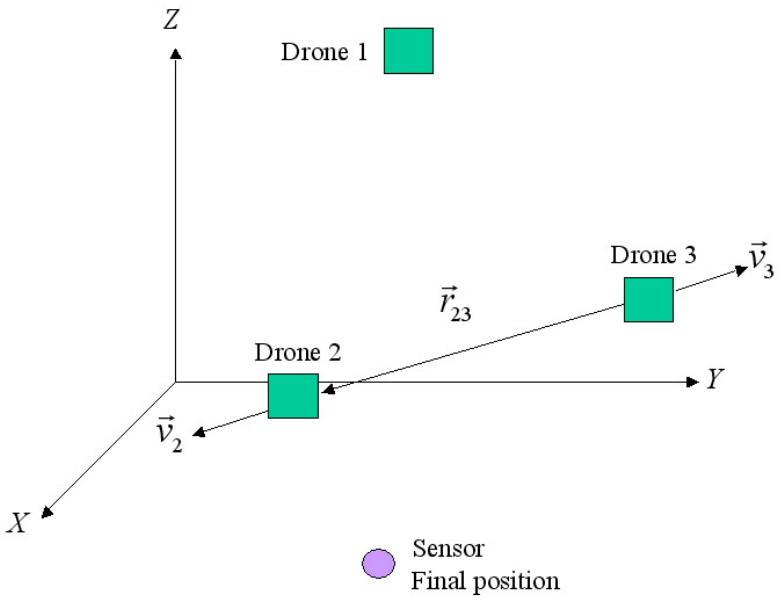

Figure 2.4: All drone craft stop

third drone craft is computed by

$$q_3 = \frac{f_{c2} r_{23}^2}{2 k_c q_2} \tag{2.18}$$

The required control force is simply determined by

$$f_{c2} = -k_d \dot{r}_{23} \tag{2.19}$$

$$\dot{r}_{23} = \dot{\boldsymbol{r}}_{23} \cdot \hat{r}_{23} \tag{2.20}$$

Finally, all spacecraft stop and another control sequence is ready to start.

There is a problem of the bang-bang control method when a sensor craft moves across the plane that is composed with three drone craft. This problem is investigated in the following sections.

2.3 Drone Plane Singularity

Three drone craft make up a plane. While controlling a sensor craft, this plane is able to translate and rotate in any direction. However, the movement of a sensor craft is limited away from the plane because the closeness of a sensor craft to the plane makes the Coulomb forces tremendously large. The singularity situation is illustrated in Figure 2.5.

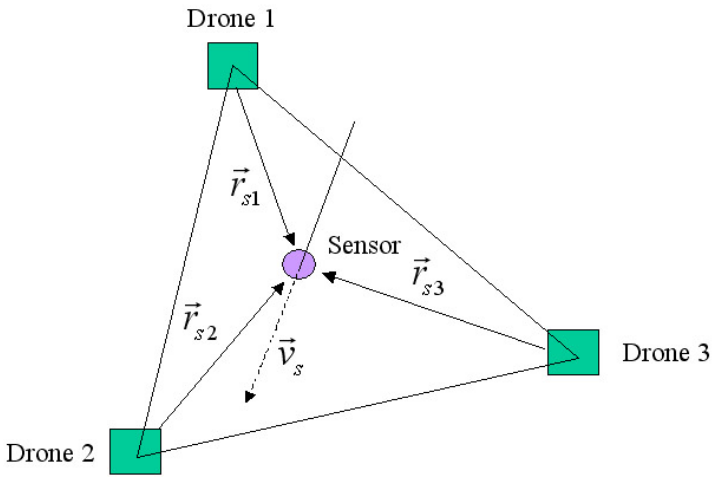

Figure 2.5: Drone plane singularity

When a sensor craft is near a drone plane, it needs dramatically large Coulomb forces to move a sensor craft to a final position. If a sensor craft is on a drone plane, there is no method to accelerate it out of the plane using Coulomb forces because Coulomb forces only exist on the plane. If a sensor craft has an initial velocity out of the plane, we can move it to a final position after waiting until the sensor craft comes out of the plane. Let us consider one sensor craft and two drone craft with the symmetry configuration as shown in Figure 2.6.

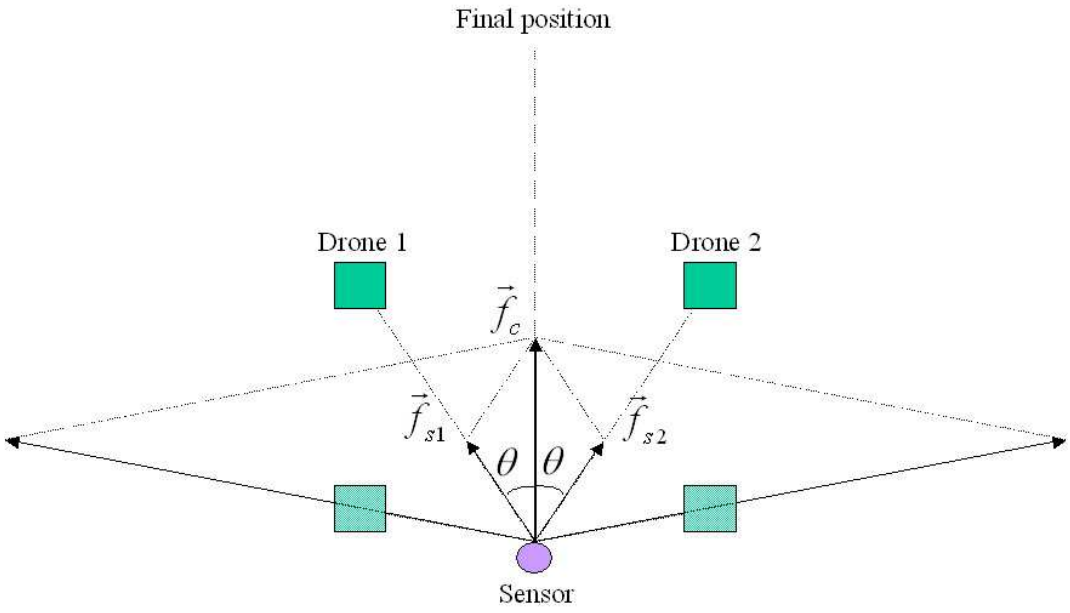

Figure 2.6: Relative forces growth

The control force of the sensor craft is written as

$$\boldsymbol{f}_c = \boldsymbol{f}_{s1} + \boldsymbol{f}_{s2} \tag{2.21}$$

and the square of the magnitude of $\boldsymbol{f}_c$ is determined by law of cosines as

$$f_{s1}^2 = f_c^2 + f_{s2}^2 - 2 f_c f_{s2} \cos\theta \tag{2.22}$$

By assuming the configuration is an isosceles triangle shape and f_{s1} and f_{s2} are the same, Eq. (2.22) can be reduced to

$$f_{s1} = \frac{f_c}{2\cos\theta} \tag{2.23}$$

Thus, relative Coulomb force between the sensor craft and the drone craft depends on the angle between these two force vectors. If θ is almost 90°, then f_{s1} should be infinity.

A sensor craft cannot be continuously controlled while passing through a drone plane because large Coulomb forces are required near the plane. We can implement a dead band using a Schmidt trigger logic to avoid abnormal charging. The size of a dead band depends on the capacity of the charging devices and the effect of charging level. In this case it is assumed that there is a charge limit.

If a sensor craft enters the dead band, the sensor craft charge needs to be zero and the sensor craft coasts without Coulomb force interaction. Three drone craft have some level of charge. They are still moving while the drone formation contracts or expands. If there is no control of the drone formation shape, drone craft may collide with others or the formation shape may not be suitable to control a sensor craft after passing a drone plane. Therefore, we need to control the formation of drone craft while a sensor craft passes through the drone plane. One method is that charges of all drone craft are set to zero to restrain the expansion or contraction of drone formation while the sensor craft flies in the dead band.

Bang-bang control type may cause drone craft to move fast as a sensor craft enters the plane because the saturation of Coulomb charge means that the highest internal forces act on each drone craft. To avoid this situation, it is required to design the bandwidth carefully or adopt a different type of control method.

2.4 Singularity Check

A singularity check process helps to avoid the singularity of a drone plane. Let $\boldsymbol{r}_{si}$ be the relative position vector between a sensor craft and the i^{th} drone craft. All relative distance vectors between the sensor craft and drone craft stay in the drone plane when the drone plane singularity happens as in Figure 2.5. Therefore, a drone plane singularity happens when Eq. (2.24) is satisfied :

$$(\hat{r}_{s1} \times \hat{r}_{s2}) \times (\hat{r}_{s2} \times \hat{r}_{s3}) = \vec{0} \tag{2.24}$$

If a sensor craft stays in a drone plane, then the cross product of $\hat{r}_{s1}$ and $\hat{r}_{s2}$ is orthogonal to the drone plane. The cross product of $\hat{r}_{s2}$ and $\hat{r}_{s3}$ is also orthogonal to the plane. Therefore the cross product of these resulting cross product vectors should be a zero vector. Using this vector calculation, Eq. (2.24) is rewritten as

$$(\hat{r}_{s1} \times \hat{r}_{s2}) \times (\hat{r}_{s2} \times \hat{r}_{s3}) = [\hat{r}_{s1} \cdot (\hat{r}_{s2} \times \hat{r}_{s3})]\hat{r}_{s2} \tag{2.25}$$

Since $\hat{r}_{s2}$ is a nonzero vector, the term in the bracket should be zero. However, the value of this term is the same as the determinant of $\boldsymbol{J}_s$ in Eq. (2.3).

If the drone plane singularity occurs, the charge of a sensor craft is turned off and the sensor craft is allowed to pass through the drone plane with zero charge. The period of turning off the charge of the sensor craft is roughly determined by the magnitude of the determinant of $\boldsymbol{J}_s$.

2.5 Simulation and Discussion

This section shows how bang-bang control method performs and illustrates its problems. Simulation parameters are set up as follows. The mass of a drone craft is 10kg and the mass of a sensor craft is 1kg. Their shapes are assumed to be spherical with a radius of 0.25 meter. Maximum charge is 1.055×10^{-6} μC. Larger gains of the PD control may increase the possibility of losing control because such gains increase the acceleration of the sensor craft and drone craft. Thus, the proportional gain for a sensor craft control is 0.001 N/m and the derivative gain is 0.05 Ns/m. The initial positions of drone craft are (1, 3, 0), (-3, 2, 0), and (1, 0, 3) m. This configuration is small but it is sufficient to check the feasibility of bang-bang control method.

2.5.1 Singularity Check Only

The initial position of a sensor craft is (0, 0, 0) m and the final position is (-0.1, 5, 3) m. All initial velocities are zero. In this simulation, the bang-bang control method works with singularity check routine. There is no other control action. Total simulation time is 1500 sec.

Figure 2.7 shows the sensor craft motion. Due to the first step of the sequential control method, the sensor craft arrives at the final position in about 200 sec. The first graph shows the inertial frame position vector components, and the second graph shows the magnitude of the distance error vector between the initial position to the final position of the sensor craft.

The third graph shows the velocity components of the sensor craft and the last graph shows the magnitude of the velocity error vector. After the distance and velocity error of the sensor craft go to zero, the drone craft will stop. The top graph of Figure 2.8 shows the distance vector components of the first drone craft and the bottom graph shows the velocity vector components. After all velocity components become zero, distance components do not change any more. The first drone stops at an arbitrary position. For the next step, the second and third drone craft would stop at the same time. Figures 2.9 and 2.10 show the motions of the second and third drone craft. After 1100 sec, they completely stop at arbitrary positions.

Figure 2.11 shows the charging status of the spacecraft. There is a jump around 50 sec, which is caused by the singularity of drone plane. Figure 2.13 shows the determinant of $\boldsymbol{J}_s$ in Eq. (2.3) during the sensor craft flight. The singularity occurs at around 50 sec. Due to the singularity check routine, the sensor craft charge is turned off and all drone craft try to stop for a short time in Figures 2.11 and 2.12. Before passing through the drone plane, the sensor craft accelerates with a positive charge and all the drone craft have negative charges. After passing through the drone plane, the sensor craft regains a maximum positive charge and decelerates by the control law. Figure 2.12 shows the magnitude of the control force acting on the sensor craft. A positive control force accelerates the sensor craft and a negative control force decelerates. The break around 50 sec is due to the singularity of the drone plane. After the sensor craft stops at the final position, the drone rest control starts to work around 650 sec. The first drone craft has a maximum charge until it is stopped. The charge of the first drone craft is turned off and the second drone craft has a maximum

charge after the first drone craft stops. During the control to stop the first drone craft, the second and third drone craft have an opposite charge to each other. This fact causes them to pull each other closer. Thus, when they try to stop, then they have same the positive charge to refrain from approaching to each other. Figure 2.14 shows the initial and final motions of the spacecraft. The initial configuration of the drone craft changes as the sensor craft moves because the inertial center of mass of the formation does not change. Thus, initial and final condition would significantly affect the configuration of the drone craft. How this phenomenon happens is shown in the following section.

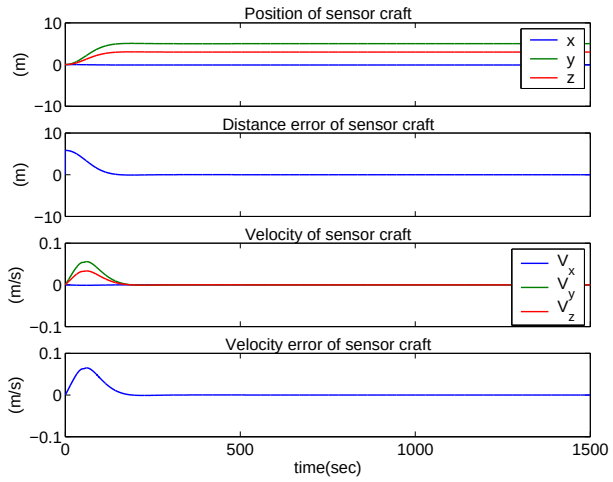

Figure 2.7: Case 1 - The velocity and position of sensor craft

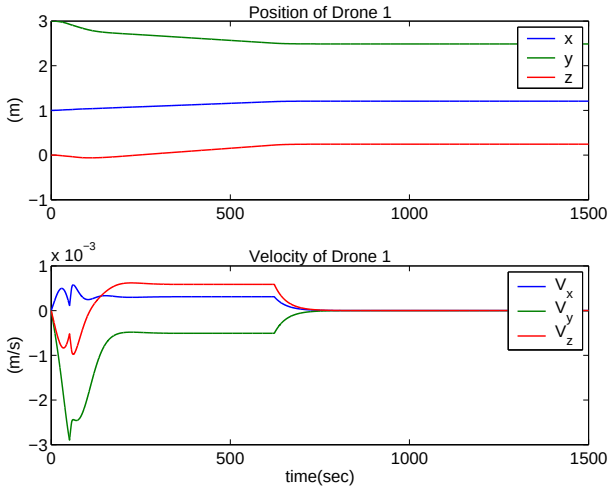

Figure 2.8: Case 1 - The velocity and position of 1st drone craft

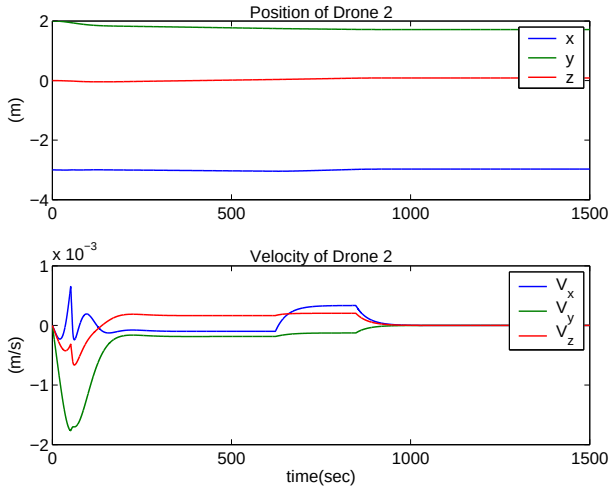

Figure 2.9: Case 1 - The velocity and position of 2nd drone craft

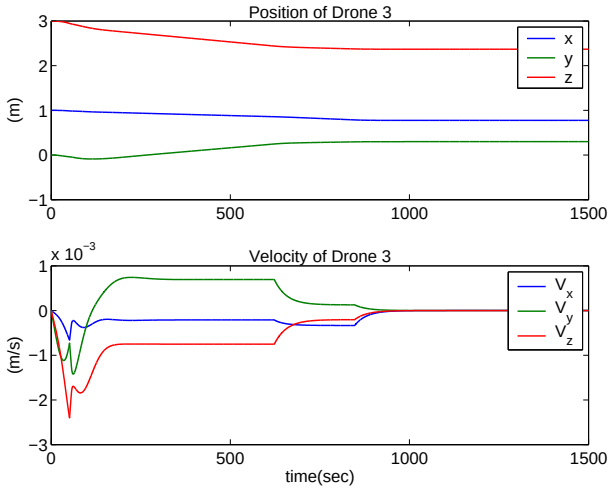

Figure 2.10: Case 1 - The velocity and position of 3rd drone craft

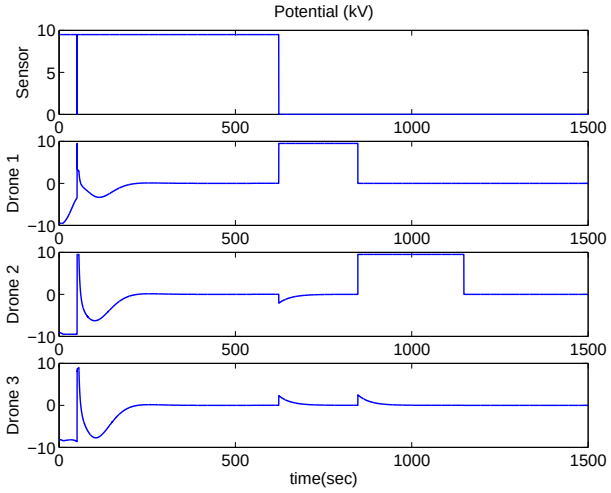

Figure 2.11: Case 1 - Charges

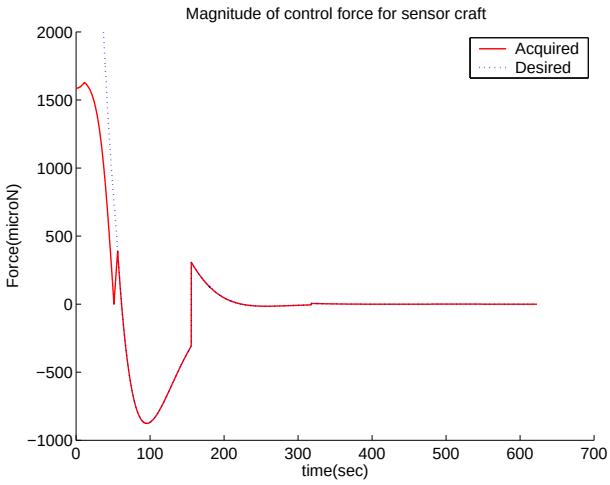

Figure 2.12: Case 1 - Coulomb control force

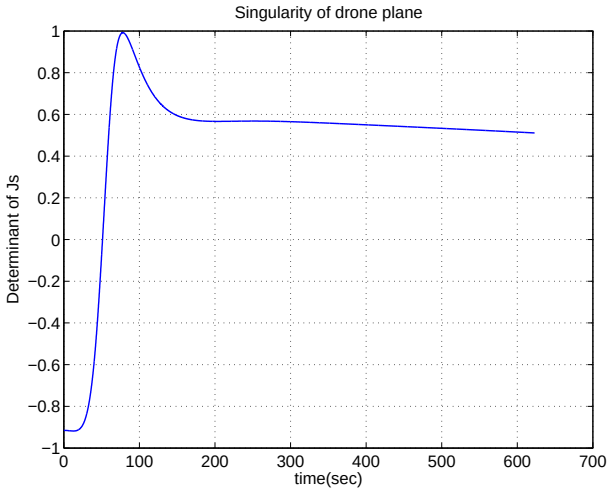

Figure 2.13: Case 1 - Singularity

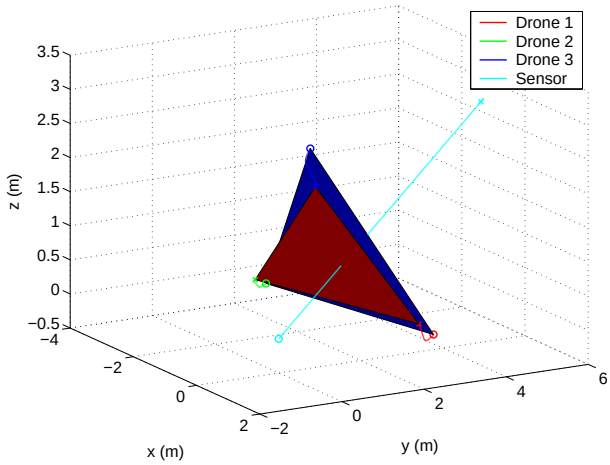

Figure 2.14: Case 1 - 3D locus

2.5.2 Collision and Formation Expansion Avoidance

Here, the initial conditions are the same as before except for the initial and final positions of the sensor craft, (2, 0, 0) m and (3, 5, 2.5) m, respectively. Figure 2.15 shows that the sensor craft arrives at the final position with overshoot. After the sensor craft stops, the first drone craft tries to stop but fails as shown in Figure 2.16. The velocity does not go to zero and the distance increases. Because the first drone craft cannot stop, the other drone craft also fail to stop as shown in Figures 2.17 and 2.18. Singularities occur twice, at around 110 sec and 420 sec, as shown in Figure 2.21. Two break responses are shown in Figure 2.19. The reason for the singularity happening twice is that the drone plane rotates while the sensor craft moves. The total angular momentum about the center of mass of the whole formation is constant and in this problem it is zero. However, the angular momentum of the sensor craft and the summation of the angular momentum of the drone craft may change with the same amount and opposite sign. The change of this angular momentum causes the drone plane to rotate. This fact is studied more specifically in Section 3.2. While the sensor craft stops at the final position, all the drone craft fail to stop because the relative Coulomb forces cannot overcome the large relative distances and the nonzero velocities between drone craft. The final configuration of the drone craft is much larger than the initial configuration. The relative distance between the first and second drone craft is nearly one hundred meters. The Coulomb force is inversely proportional to the square of the relative distance as Eq. (1.2). The Coulomb force of the relative distance of one hundred meters is four percent of the Coulomb force of the relative distance of twenty

meters. Therefore, as the relative distance increases, the Coulomb force decreases and we may lose control of the relative velocity between drone craft. To avoid these phenomena, collision and formation expansion avoidance control strategies are required.

The collision and formation expansion avoidance control is simple. The lower and upper limits of the relative distance need to be determined. When the relative distances between the drone craft exceed the predetermined limits, the charge of the sensor craft is turned off and the charges of the drone craft related with such distances are only turned on with maximum value to increase or decrease relative distances. In the following simulation, initial conditions are the same as the previous setting. In addition, the collision and formation expansion avoidance control method is set to work during the sensor craft coasting period. As can be seen from Figures 2.23 through 2.26, after the sensor craft arrives at the final position, all drone craft stop within several meters. The collision and formation expansion avoidance control works properly between 380 sec and 440 sec as shown in Figure 2.27. Because the first drone and second drone approach each other excessively, positive maximum charges are produced to repel each other. During that time, there is no control force in Figure 2.28. In this way, the drone plane singularity is changed as seen from comparing Figure 2.21 to Figure 2.29. Though the control purpose is satisfied, the sensor craft arrives at the final position and all drone craft stop, the final configuration of drone craft may not be suitable to control the sensor craft to move to a new desired position. This topic is left for further study.

Continuous control action during a sensor craft flight can accelerate a sensor craft. In

addition, it can increase the relative velocity between a drone craft and another drone craft. This effect changes the formation shape of the drone craft to an unwanted shape, because there is no control of the drone craft formation during the process of sensor craft control. It is possible to lose the reposition control of a sensor craft with unwanted drone craft formation shape and the velocities of drone craft, especially when the flight path line of the sensor craft passes through the outside of the drone craft triangle. Therefore, the initial and final conditions should be carefully determined.

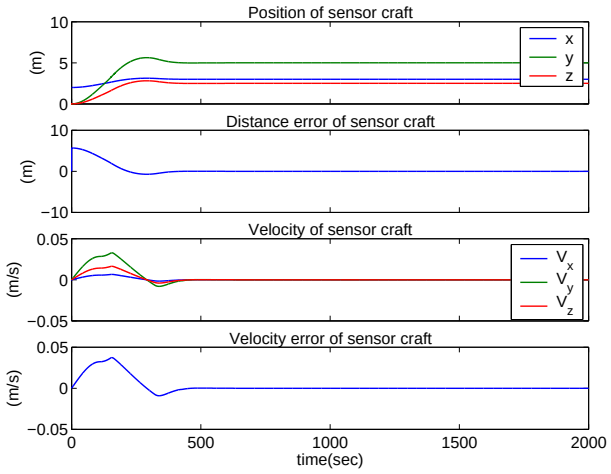

Figure 2.15: Case 2.1 - The velocity and position of sensor craft

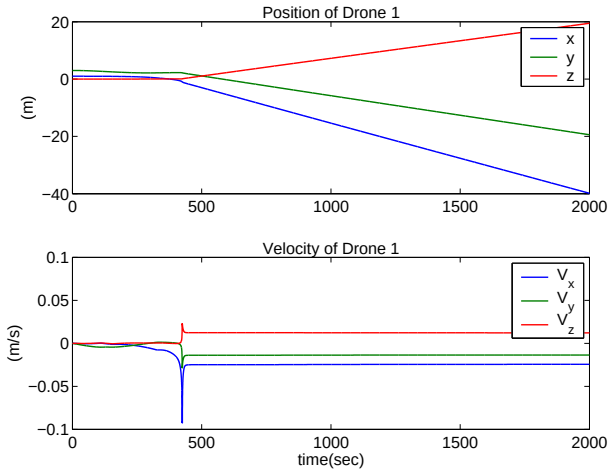

Figure 2.16: Case 2.1 - The velocity and position of 1st drone craft

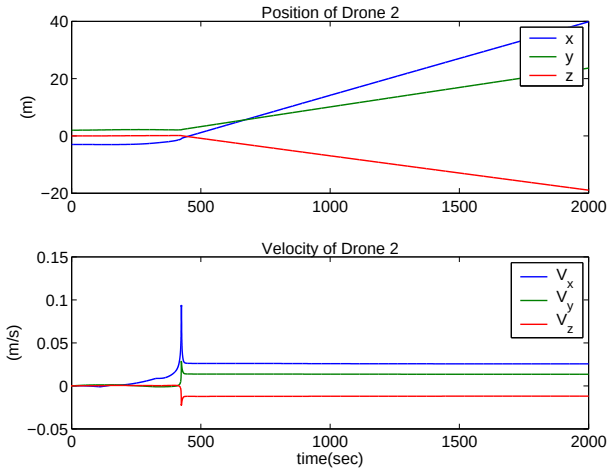

Figure 2.17: Case 2.1 - The velocity and position of 2nd drone craft

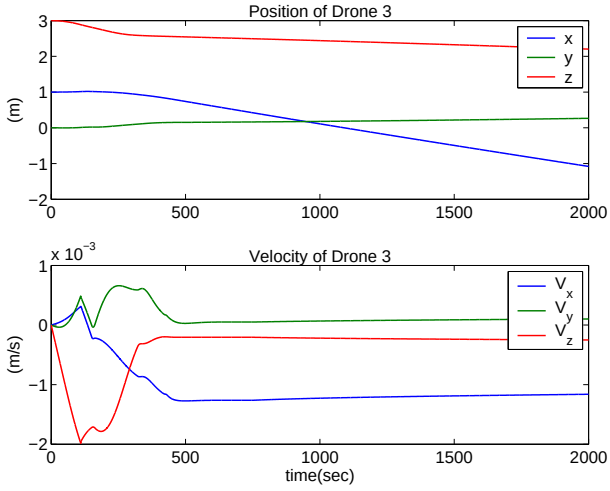

Figure 2.18: Case 2.1 - The velocity and position of 3rd drone craft

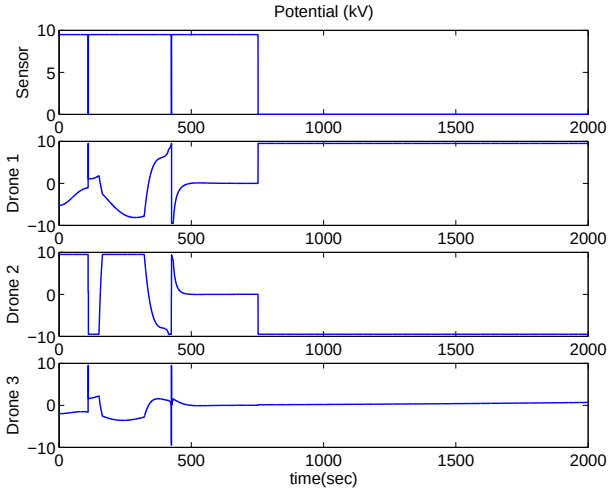

Figure 2.19: Case 2.1 - Charges

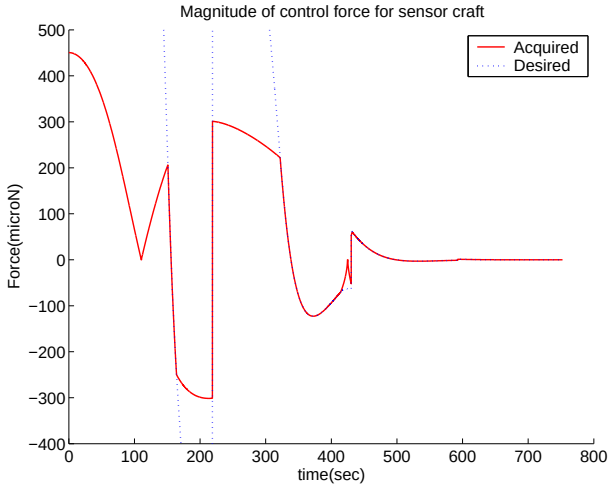

Figure 2.20: Case 2.1 - Coulomb control force

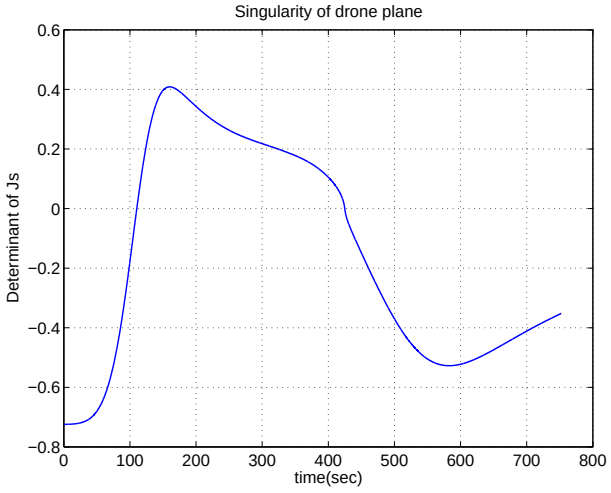

Figure 2.21: Case 2.1 - Singularity

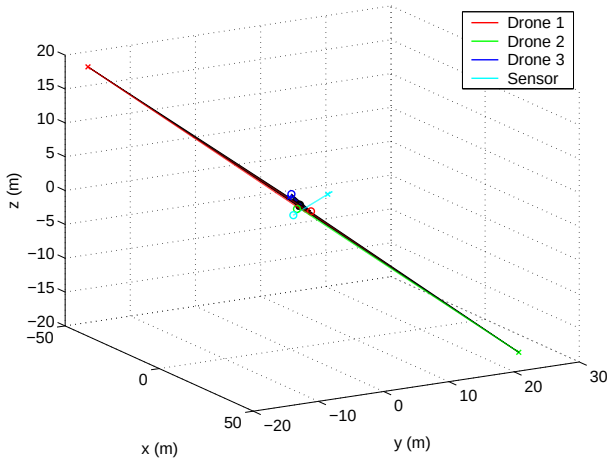

Figure 2.22: Case 2.1 - 3D locus

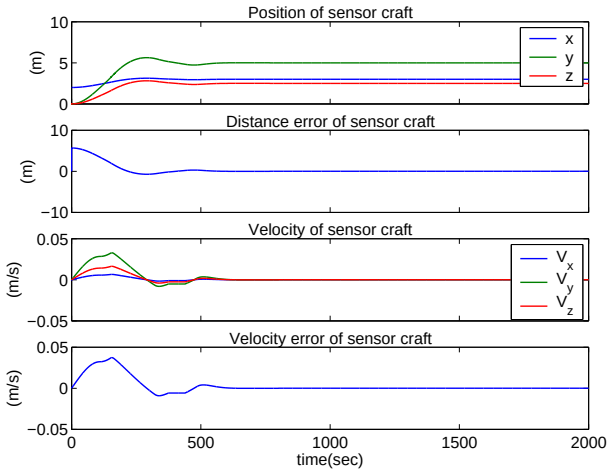

Figure 2.23: Case 2.2 - The velocity and position of sensor craft

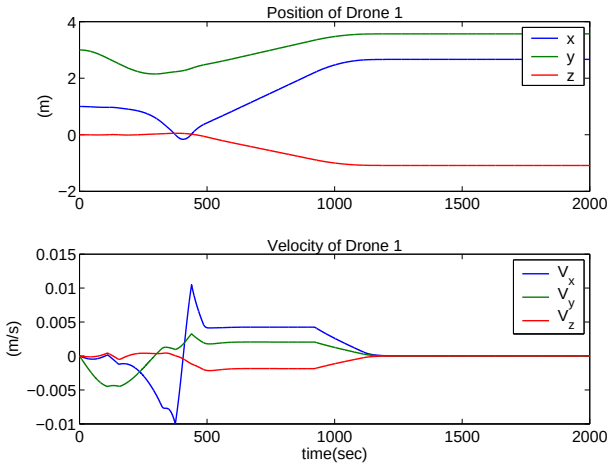

Figure 2.24: Case 2.2 - The velocity and position of 1st drone craft

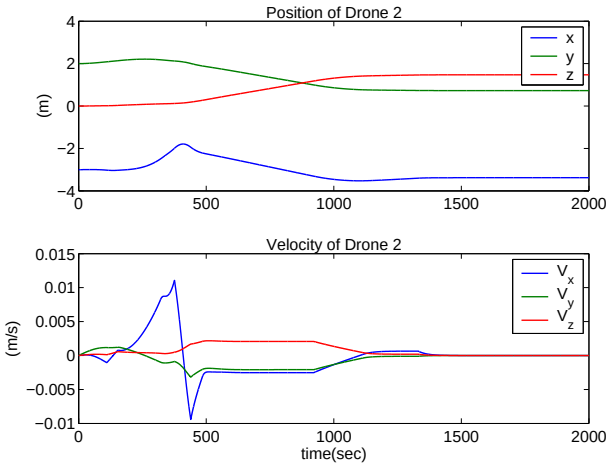

Figure 2.25: Case 2.2 - The velocity and position of 2nd drone craft

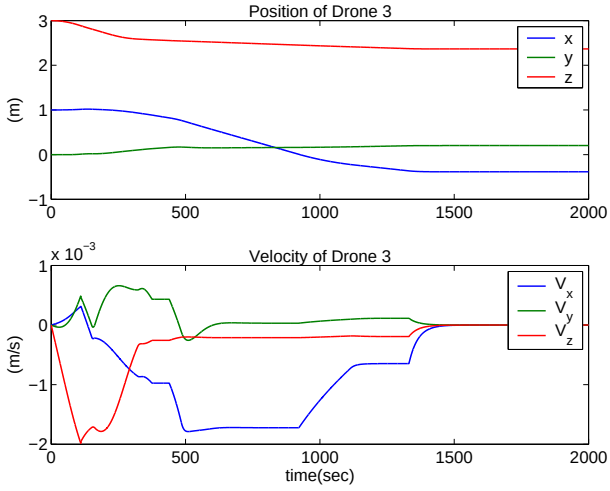

Figure 2.26: Case 2.2 - The velocity and position of 3rd drone craft

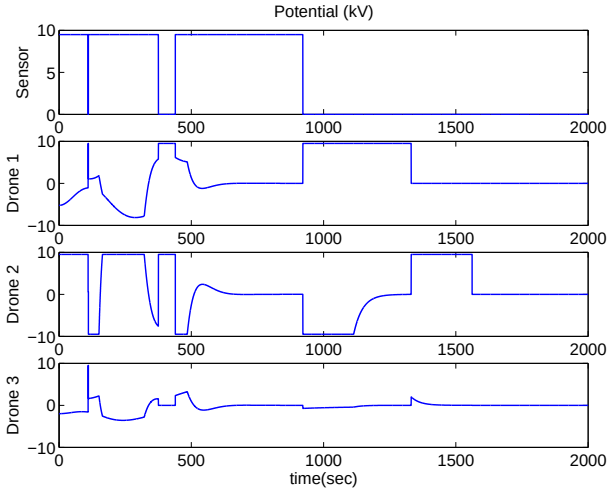

Figure 2.27: Case 2.2 - Charges

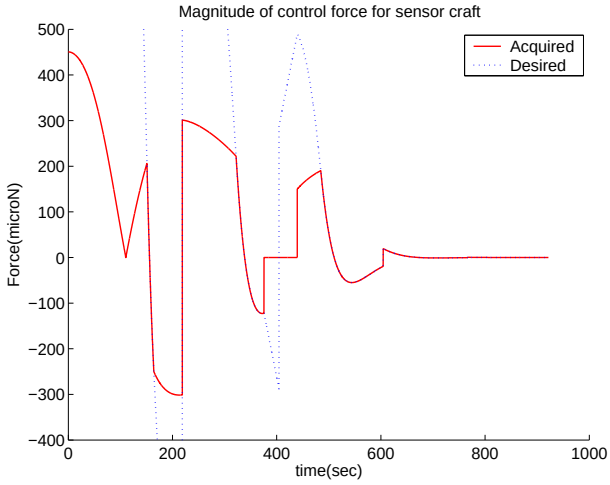

Figure 2.28: Case 2.2 - Coulomb control force

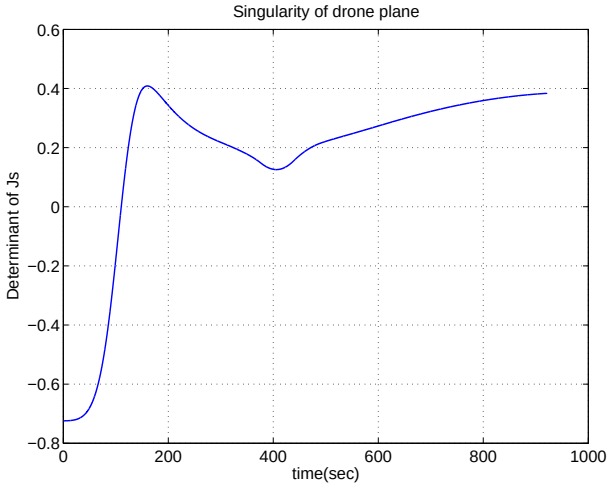

Figure 2.29: Case 2.2 - Singularity

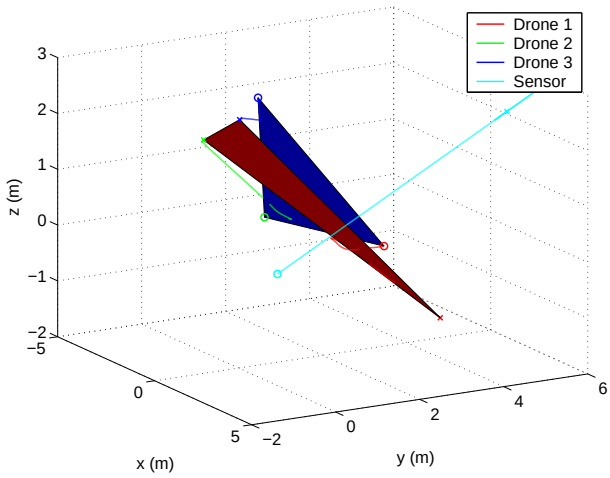

Figure 2.30: Case 2.2 - 3D locus

2.5.3 Large Configuration

The possibility of losing control increases as the flight distance of a sensor craft increases. In this simulation, the initial configuration of drone craft is expanded to twice the size of the previous setting and the flight distance of a sensor craft is increased to dozens of meters. Spacecraft shape is assumed to be sphere with one meter radius. The initial position of the sensor craft is (0, 20, 0) m and the final position is (0, -20, 0) m. The initial positions of drone craft are (0, 0, 8) m, (6.9282, 0, -4) m, and (-6.9282, 0, -4) m, respectively. These positions compose an equilateral triangle with the center at (0, 0, 0) m. The relative distance between drone craft is 12 m and the flight distance of the sensor craft is 40 m. Other parameters are the same as Section 2.5.2.

As can be seen from Figures 2.31 through 2.34, the sensor craft passes by the final position and cannot come back, the drone craft are not able to control the sensor craft, and the drone craft formation keeps expanding. The singularity of the drone plane happens only once at around 720 sec in Figure 2.37. The sensor craft accelerates until approaching the final position and decelerates after passing the final position with maximum charging level. At that time, the desired control force is much larger than the actual available control force. These responses are shown in Figures 2.35 and 2.36. Insufficient control force is caused by the configuration of spacecraft and velocities at that time. Figure 2.38 shows that the effort of the drone craft to pull the sensor craft causes the formation of drone craft to become much larger. Increasing the maximum charge of the sensor craft and turning on the collision and formation expansion avoidance control does not help to control the system. It may be

proposed that if the formation of the drone craft is restricted during a sensor craft flight, then the control object can be achieved. This topic is discussed in the following chapter.

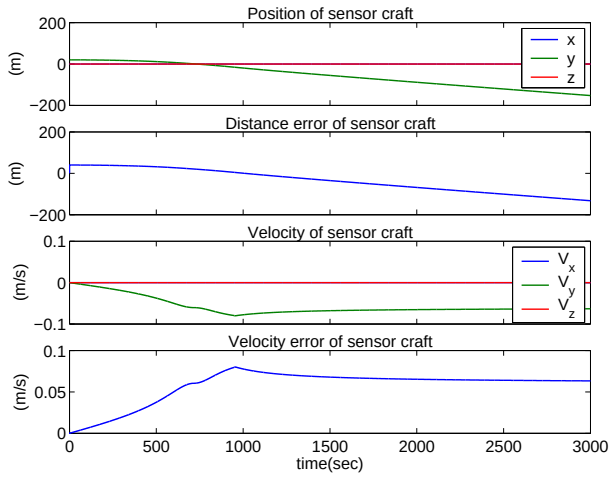

Figure 2.31: Case 3 - The velocity and position of sensor craft

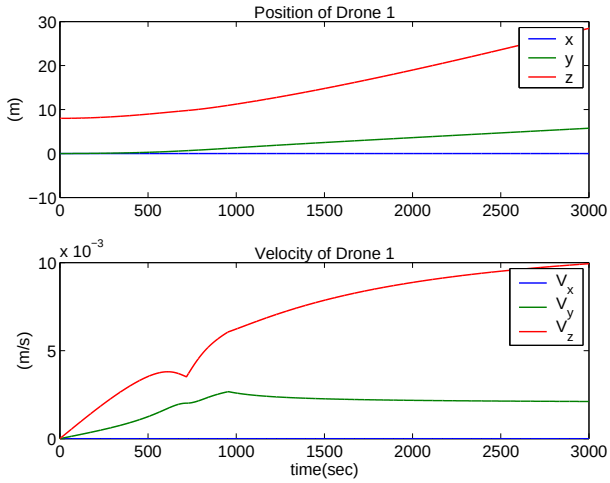

Figure 2.32: Case 3 - The velocity and position of 1st drone craft

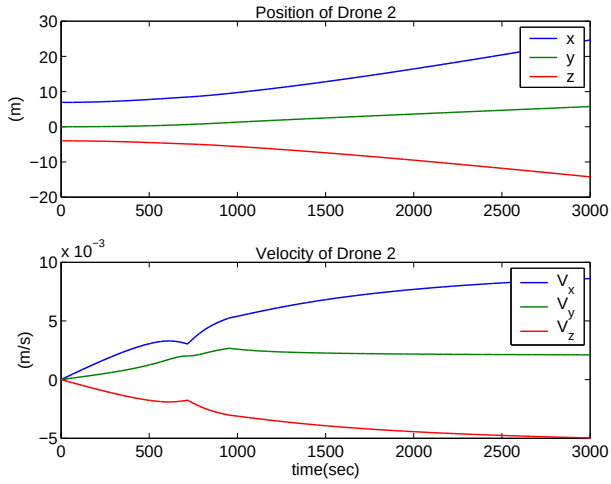

Figure 2.33: Case 3 - The velocity and position of 2nd drone craft

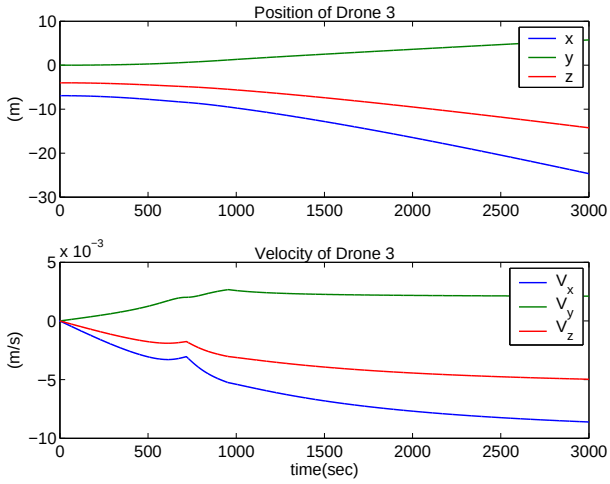

Figure 2.34: Case 3 - The velocity and position of 3rd drone craft

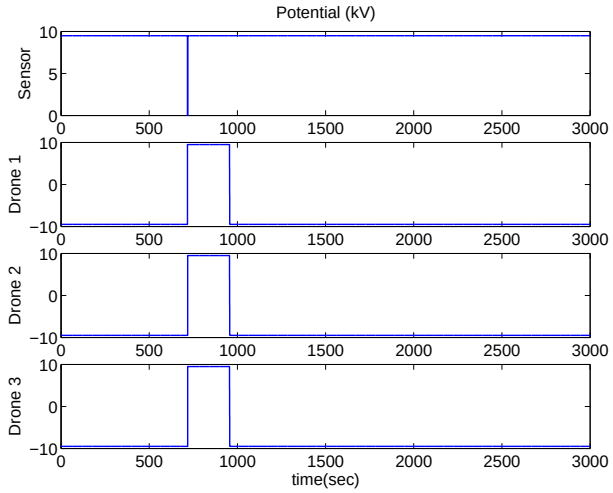

Figure 2.35: Case 3 - Charges

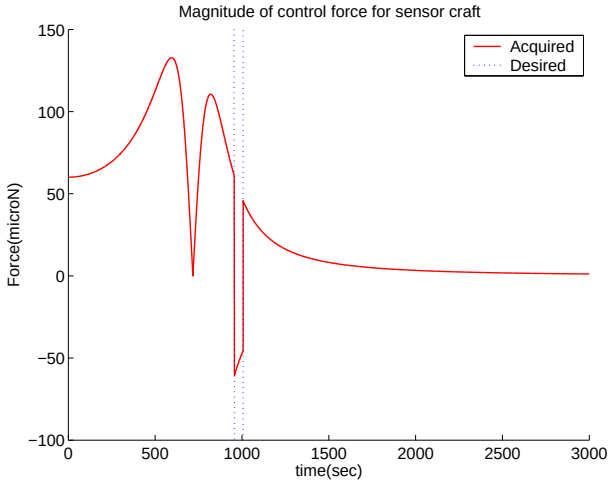

Figure 2.36: Case 3 - Coulomb control force

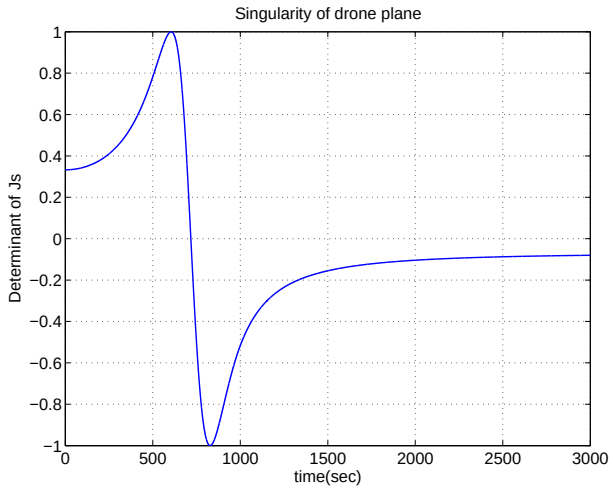

Figure 2.37: Case 3 - Singularity

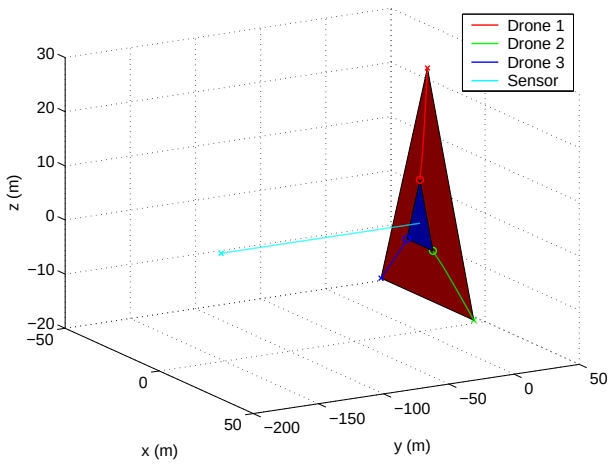

Figure 2.38: Case 3 - 3D locus

Chapter 3

Bang-Coast-Bang Control

Generating a continuous control force onto the sensor craft causes the drone craft formation to expand or contract severely, as illustrated through the numerical examples in the previous chapter. The relative forces among the drone craft increase the relative speed of drone craft. The undesired configuration of the drone craft formation may result in a loss of control of the sensor craft. To avoid this problem, a sensor craft accelerates for a short time to get the required coast speed and direction (bang period), and then flies without any control across the drone plane (coast period). Finally, as the sensor craft approaches the final position (second bang period) and enters into the control boundary, it will decelerate to arrive and stop at the final position. During the sensor craft coast period, the drone craft can be reconfigured for better control performance without influencing the sensor craft motion. The initial control force is not constant because the control force may vary with the relative distances and the saturation of charges. In contrast with Figure 2.1, the solid force arrows

in the Figure 3.1 are smaller, indicating smaller control forces being used to accelerate the sensor craft. The dotted line means that there is no control force acting on the sensor craft. This line forms the coasting line of the sensor craft.

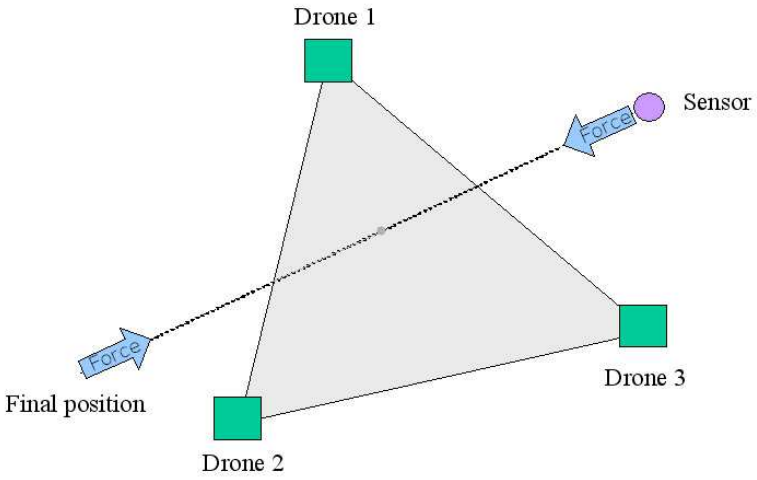

Figure 3.1: Bang-coast-bang concept

To achieve this control, the coasting velocity and the control boundary should be predetermined by reference profiles. The flying period of the sensor craft can be easily adjusted.

3.1 Reference Profile

A sensor craft acquires a predetermined constant speed after the initial acceleration process. Because there is no external force acting on the sensor craft, it is easy to predict when the sensor craft arrives at the final position. The distance and velocity profile can be used to stop the sensor craft at the final position with a constant deceleration. A deceleration can be

calculated from the constant coasting speed and the operation time of deceleration. In this case a constant deceleration is applied and the velocity profile is described as a first order polynomial. A corresponding distance profile is shown in the type of quadratic polynomial because distance is integration of velocity. The velocity is shown in Figure 3.2.

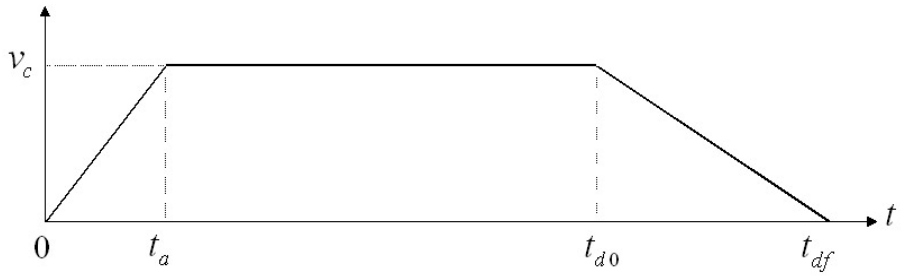

Figure 3.2: Reference velocity profile

A sensor craft will accelerate to achieve the coasting speed, v_c, by t_a. The time between t_a and t_{d0} is the coasting period. Deceleration starts in t_{d0} and ends by t_{df}. The corresponding distance profile is shown in Figure 3.3.

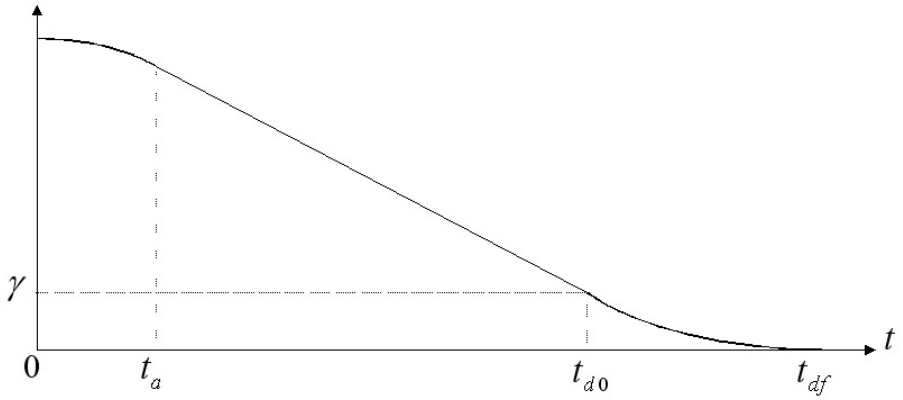

Figure 3.3: Reference distance profile

The initial value of the distance is the initial distance error between sensor craft position and the final position. Therefore, distance profile looks like a decreasing function.

Using the coasting velocity and deceleration duration time, t_d, we can determine the velocity and distance profiles which are expressed as

$$v_p = v_c + a_{dec}(t - t_{d0}) \tag{3.1}$$

$$d_p = \gamma - v_c(t - t_{d0}) - \frac{a_{dec}(t - t_{d0})^2}{2} \tag{3.2}$$

where t_{d0} is deceleration starting time, γ is the band of deceleration, and a_{dec} is a constant deceleration. The parameters, γ and a_{dec}, are determined by Eqs. (3.1) and (3.2).

$$a_{dec} = -\frac{v_c}{t_d} \tag{3.3}$$

$$\gamma = \frac{v_c t_d}{2} \tag{3.4}$$

The control law used in this study is a PD control type as described by Eq. (2.9). A constant deceleration force is the feedforward input. This control force is used to decrease the sensor craft velocity, but cannot be used to adjust the difference between profile value and error. Therefore, a feedback control is still required and the feedforward control should be added. Thus, the final augmented control force is described as

$$f_{caug} = k_p e_{aug} + k_d \dot{e}_{aug} + f_{dec} \tag{3.5}$$

where

$$e_{aug} = e - d_p \tag{3.6}$$

$$\dot{e}_{aug} = \dot{e} + v_p \tag{3.7}$$

$$f_{dec} = m_s a_{dec} \tag{3.8}$$

Although d_p, v_p, and f_{dec} are set to zero after t_{df}, the error velocity and distance of the sensor craft could not be zero and overshoot can be expected. Therefore, additional time is required to allow the sensor craft to completely stop at the final position.

3.2 Angular Momentum of Formation

The angular momentum of the formation is constant because there is no external force acting on the the formation.

$$\boldsymbol{H}_t(t) = \boldsymbol{H}_s(t) + \boldsymbol{H}_d(t) = \text{const} \tag{3.9}$$

where $\boldsymbol{H}_t(t)$ is the total angular momentum of the whole system, $\boldsymbol{H}_s(t)$ is the angular momentum of a sensor craft, and $\boldsymbol{H}_d(t)$ is the summation of the angular momentum of the drone craft.

All spacecraft have no initial velocity. Therefore, $\boldsymbol{H}_t(t)$ must remain zero at all times. However, $\boldsymbol{H}_s(t)$ and $\boldsymbol{H}_d(t)$ may have nonzero values after all craft start to move. If the center of mass of the formation, which is the reference point of angular momentum, lies on the coasting line of a sensor craft, then the angular momentum of the sensor craft and the summation of the angular momentum of the drone craft does not change. The angular

momentum of a sensor craft about the center of mass of the formation is expressed as

$$\boldsymbol{H}_s(t) = (\boldsymbol{r}_s - \boldsymbol{r}_c) \times m_s \dot{\boldsymbol{r}}_s \tag{3.10}$$

where $\boldsymbol{r}_c$ is the position vector of the center of mass of the formation. If the vector difference, $\boldsymbol{r}_s - \boldsymbol{r}_c$, and $\dot{\boldsymbol{r}}_s$ lie on the coasting line, then the cross product of these terms is zero. Thus,

$$\boldsymbol{H}_s(t) = 0 \Rightarrow \boldsymbol{H}_d(t) = 0 \quad \text{for all time} \tag{3.11}$$

This means that the orientation of the drone plane is fixed while all craft are moving and the drone plane does not rotate in inertial frame. Figure 3.4 shows this fact. The initial configuration of drone craft is an equilateral triangular shape and the coasting line passes through the center of mass of the formation. As can be seen from Figure 3.4, every drone plane is parallel to each other. Because the drone can propel themselves through inertial

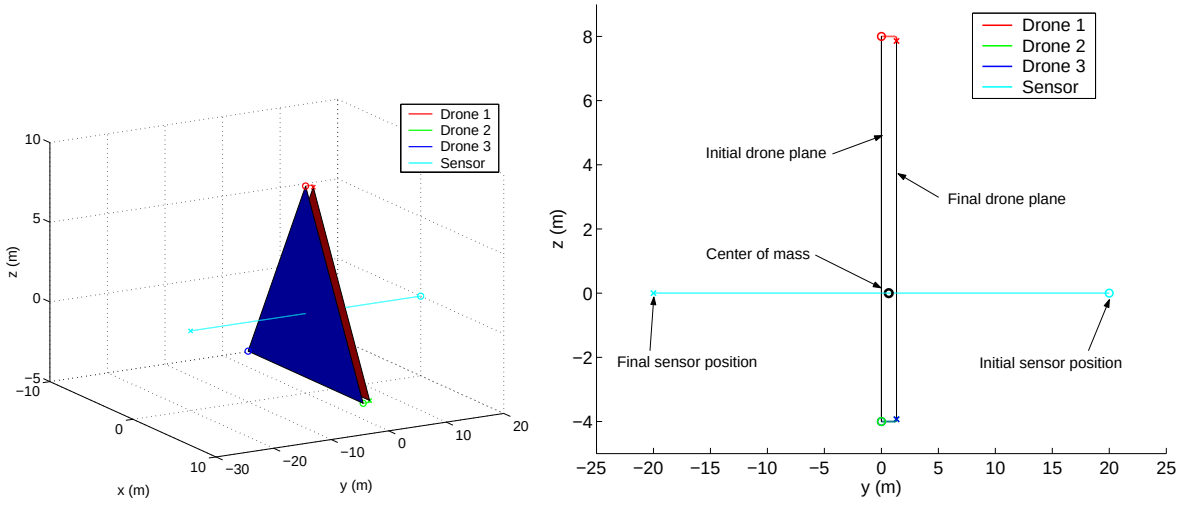

Figure 3.4: Drone plane translation

space, they should first aligned themselves such that their center of mass point is located on the sensor craft flight path. Doing so will guarantee that the drone plane does not rotate and will allow the drone motion to be cancelled during the coast period of the sensor craft.

In contrast, if the center of whole formation is out of the coasting line, then each angular momentum has a nonzero value as shown in Figure 3.5, and the drone plane starts to rotate in Figure 3.6. The initial configuration is same as Figure 3.4 but the final sensor position is different. Figure 3.5 shows that angular momentums does vary as the sensor craft moves. The magnitude of $\boldsymbol{H}_s(t)$ increases during the acceleration period, stays at the constant value during coasting period, decreases during deceleration period and finally goes to zero. The time history of the magnitude of $\boldsymbol{H}_d(t)$ shows exactly the opposite response with the same absolute value.

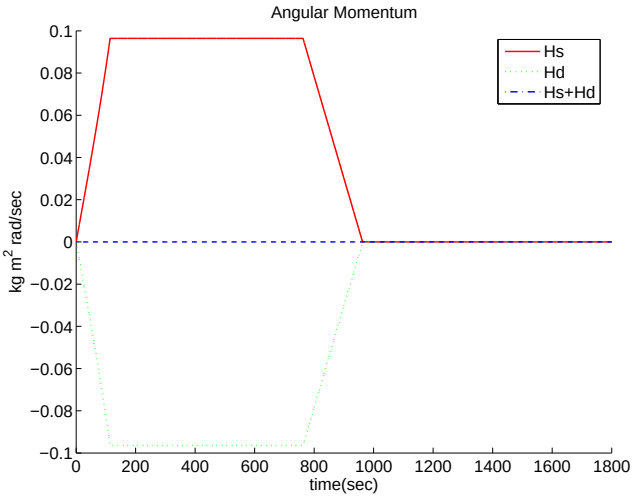

Figure 3.5: Angular momentum change

In Figure 3.6 the center of mass of the formation is not located on the coasting line. $\boldsymbol{H}_s(t)$ has a left clockwise direction and $\boldsymbol{H}_d(t)$ has a right clockwise direction. This fact causes the drone plane to rotate during the sensor craft moving.

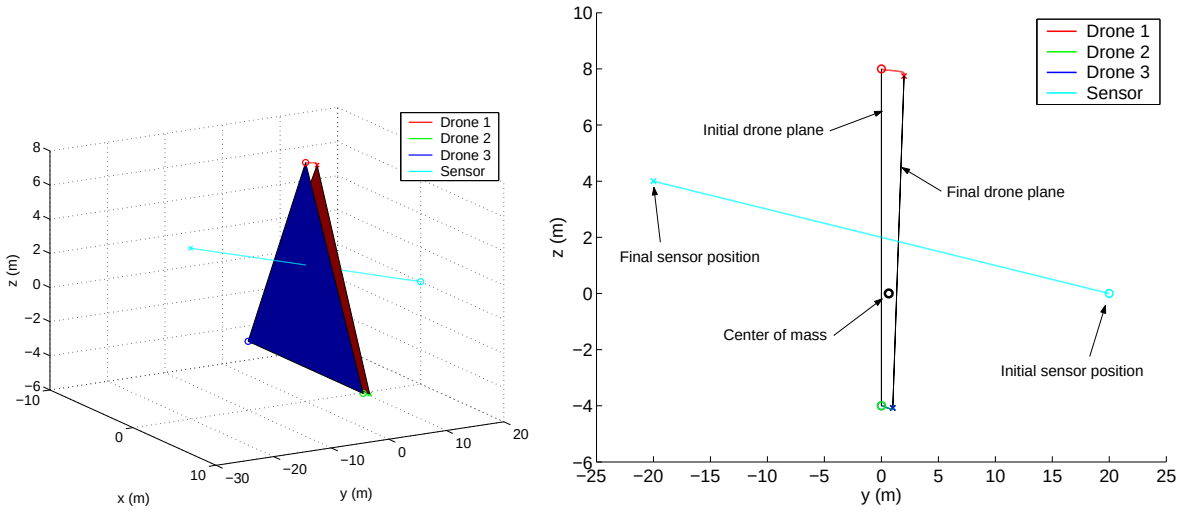

Figure 3.6: Drone plane rotation

Due to this fact it is difficult to use the drone rest control on the drone plane in the following section. If the drone plane does not rotate, then if a drone craft stops on the drone plane, it will keep the position on the plane. If the drone plane rotates, then centrifugal force acts on the temporarily arrested drone craft and it can not stay a certain point on the plane without any control force. In the sequential control process, the charge of a drone craft is turned off after it becomes rest. Therefore, when the drone plane rotates the charge of the drone craft is repeatedly turned on and off. Consequently, first drone craft can not have zero velocity on the drone plane and other drone craft still try to stop it but they fail to do so. Such drone

rest control is only valid when the center of a whole formation lies on the line of sight from the initial position of a sensor craft to the final position. The drone plane does not rotate and has a linear velocity only in this condition.

3.3 Drone Control during Sensor Craft Coasting Period

While a sensor craft is coasting without any Coulomb control force, the drone craft should be controlled to avoid collision or formation expansion. Since there is no charge on a sensor craft while it is coasting, the drone craft control is limited on the drone plane. Although control forces only act on the drone plane, all drone's inertial movement is not confined on the plane, because the plane is not fixed in inertial space. Therefore, the velocity component of a drone craft which is projected on the drone plane will need to be zero and the orthogonal velocity to the plane will be nonzero and the plane will keep moving. The projection of a drone velocity vector is computed using relative distance unit vectors. All relative distance unit vectors always stay on the drone plane. The projection velocity vector of a drone can be decomposed using two relative distance unit vectors, though they are not necessarily orthogonal to each other. Thus, each projection velocity vector is described by

$$\boldsymbol{v}_{dp1} = (\boldsymbol{v}_1 \cdot \hat{r}_{12})\hat{r}_{12} + (\boldsymbol{v}_1 \cdot \hat{r}_{13})\hat{r}_{13} \tag{3.12}$$

$$\boldsymbol{v}_{dp2} = (\boldsymbol{v}_2 \cdot \hat{r}_{21})\hat{r}_{21} + (\boldsymbol{v}_2 \cdot \hat{r}_{23})\hat{r}_{23} \tag{3.13}$$

$$\boldsymbol{v}_{dp3} = (\boldsymbol{v}_3 \cdot \hat{r}_{31})\hat{r}_{31} + (\boldsymbol{v}_3 \cdot \hat{r}_{32})\hat{r}_{32} \tag{3.14}$$

where the subscript, dp , means drone plane. One of the projection velocity vectors is displayed in Figure 3.7.

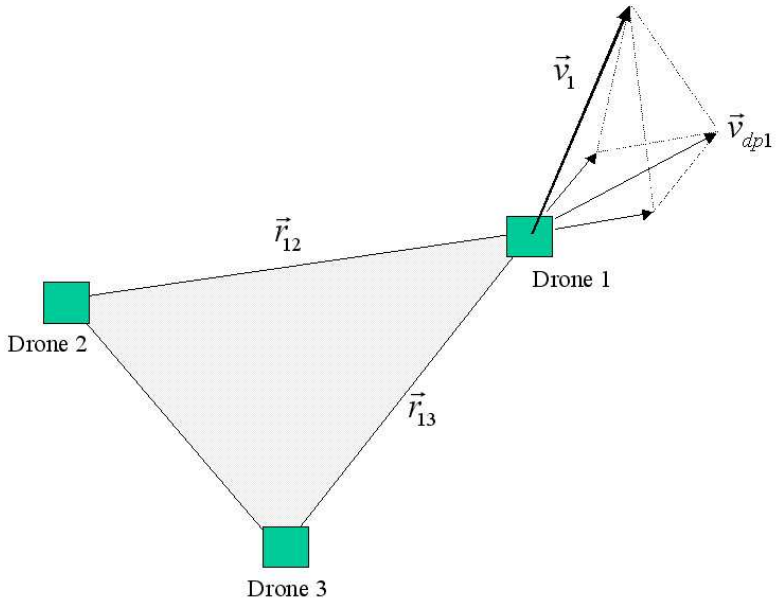

Figure 3.7: Projection velocity on the drone plane

The control objective of this stage is to make the magnitude of each projection velocity vector zero. The control logic is similar to that of Section 2.2. The only difference is that the projection velocity vector is used instead of the velocity vector of a drone craft.

3.4 Simulation and Discussion

All initial conditions are the same as those of Section 2.5.3, except for the following parameters. To increase the acceleration of a sensor craft, the maximum charge of the sensor craft

is set to 1.055×10^{-5} μC. This value is ten times that of the maximum charge of a drone craft. In addition, the proportional gain for a sensor craft control is 0.002 N/m and the derivative gain is 0.09 Ns/m and these values are almost twice those of the previous setting. The deceleration of the sensor craft acts for 200 sec.

3.4.1 Bang-Coast-Bang Flight with PD Control

Section 2.5.3 shows that it was difficult to control the sensor craft and drone craft with the initial configuration using the earlier Bang-Bang control strategy. In this simulation, the control purpose is achieved by using the sensor craft coasting period. The predetermined coasting speed is 5 cm/sec and the charge of the sensor craft is turned on again when distance error is under 5 m.

Figures 3.8 through 3.11 show the results. The sensor craft accelerates during the first 90 sec and the drone craft also accelerates at the same time. To produce the maximum acceleration, the desired control force is set to one newton. Due to the charge saturation and the relative geometry of spacecraft, the acquired force in the first part is not constant, but maximum control force at that instant time as shown in Figure 3.13. After acquiring the predetermined coasting speed of 5 cm/sec, all charges of the spacecraft are turned off until the distance error of the sensor craft becomes 5 m. During the coasting period, the velocities of the spacecraft are constant. The break responses around 760 sec in Figures 3.8 through 3.11 are caused by turning on the charges of all spacecraft and charging levels are

determined by the PD control law. Due to the charge saturation, velocities of the drone craft suddenly increase, but the magnitude of them are smaller than that of the sensor craft. Thus, it is easily expected that the final configuration of the drone craft would not expand substantially. Figure 3.12 shows the charging status of the spacecraft. Until the sensor craft stops, the charging status of the drone craft is the same and all the drone craft push each other because the initial configuration of drone craft is an equilateral triangle shape and the coasting line of the sensor craft passes through the center of mass of the whole system. After turning off the charge of the sensor craft, the second and third drone craft have the opposite sign of the charge of the first drone craft to stop the first drone craft. After stopping the first drone craft, the second and third drone craft have also the opposite sign of the charge with respect to each other. As explained in Section 3.2, the angular momentum of the sensor craft about the center of mass of the whole system is zero at all times and the summation of the angular momentum of the drone craft is also zero correspondingly. Comparing Figure 3.15 with that of Figure 2.38, the final configuration did not expand very much.

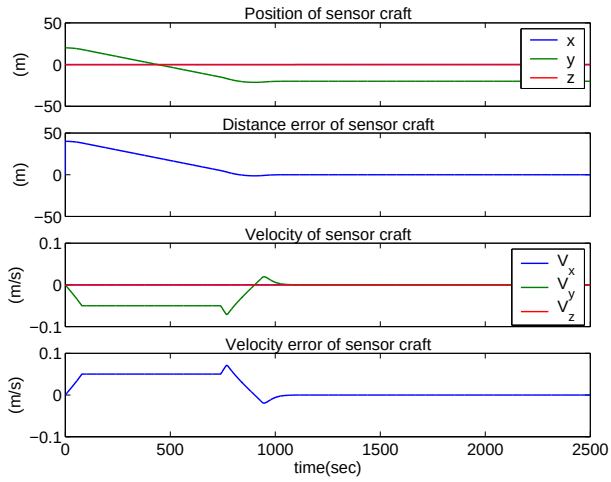

Figure 3.8: Case 4 - The velocity and position of sensor craft

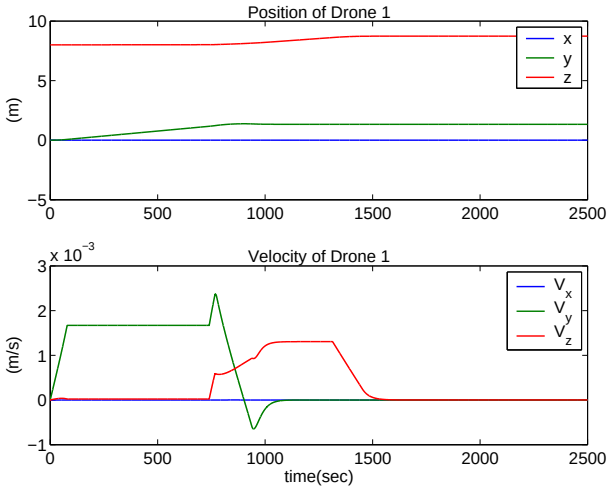

Figure 3.9: Case 4 - The velocity and position of 1st drone craft

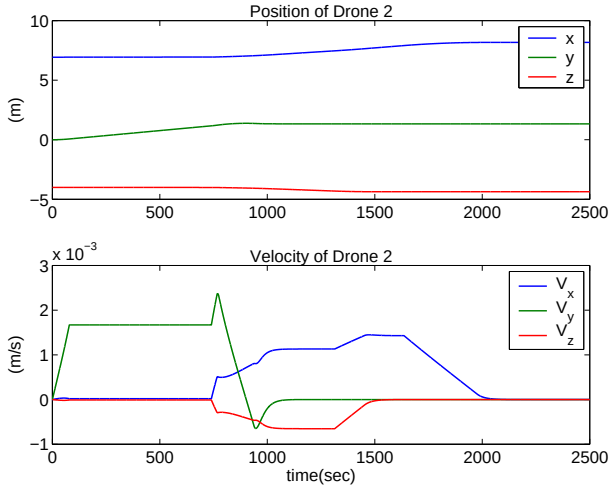

Figure 3.10: Case 4 - The velocity and position of 2nd drone craft

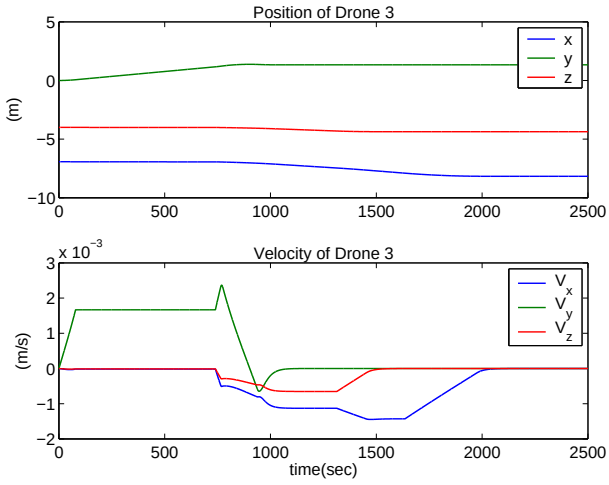

Figure 3.11: Case 4 - The velocity and position of 3rd drone craft

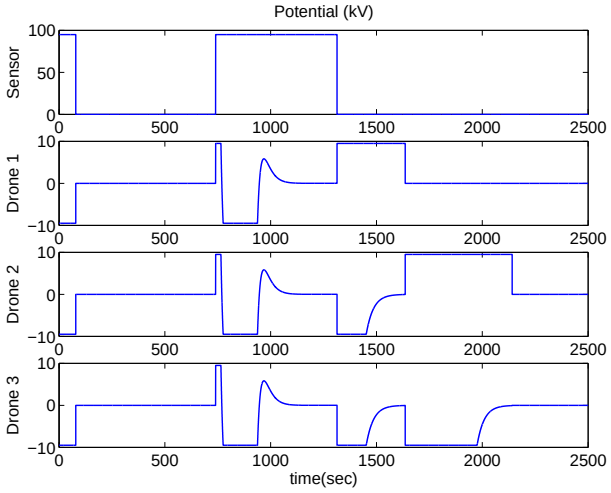

Figure 3.12: Case 4 - Charges

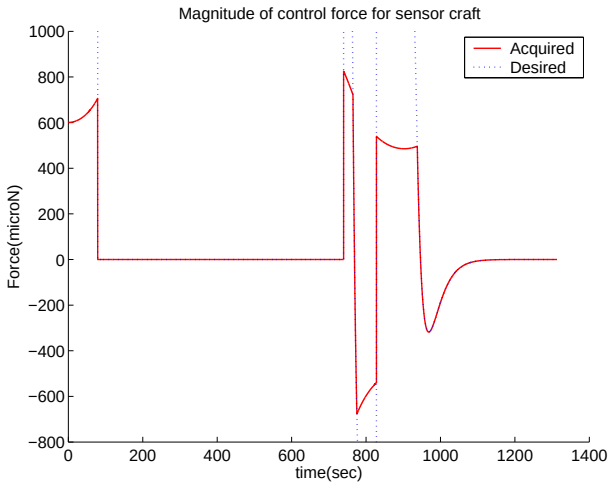

Figure 3.13: Case 4 - Coulomb control force

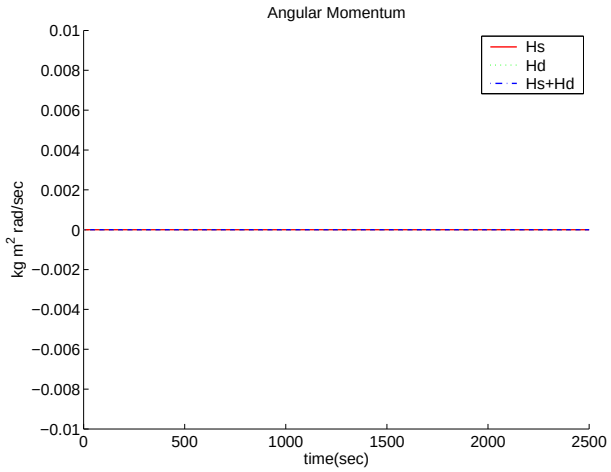

Figure 3.14: Case 4 - Angular momentum

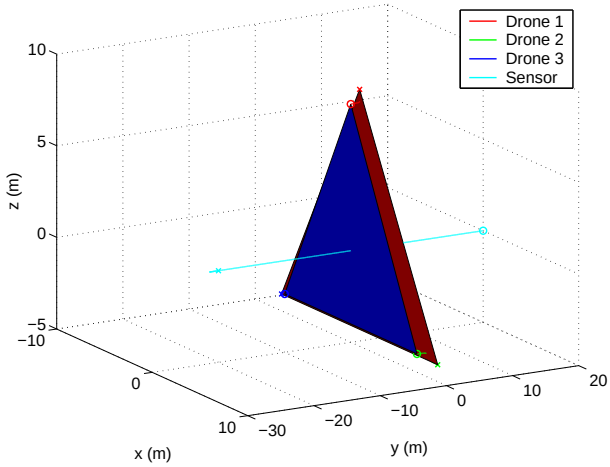

Figure 3.15: Case 4 - 3D locus

3.4.2 Effect of the Reference Profile

An overshoot is detected in the previous results, although the velocity of the sensor craft was 5 cm/sec. Reference profiles can help to coordinate the response of the sensor craft smoothly while minimizing overshoot. The drone craft rest control during the coasting period will stop the expansion of drone formation.

The second and bottom plots of Figure 3.16 are similar to Figure 3.3 and 3.2 respectively. This system also has some overshoot, but it is smaller than the previous result. During the coasting period, all the drone craft stopped on the drone plane. As can be seen from Figures 3.17, 3.18, and 3.19, velocity components of x and y axes are maintained to be zero because the drone plane is always orthogonal to the inertial y axis. Due to the initial conditions, there is no rotation of the drone plane. Figures 3.20 and 3.21 clearly show the reference profile effect and the drone rest control during the coasting period. After acquiring the required coasting speed due to the maximum control forces, the first drone tries to stop using the other two drone craft. This sequence looks similar to the control action after the sensor craft stopped. The desired control forces are zero during the coasting period and constant during the decelerating period. Figure 3.21 shows the desired and acquired control force is -250 N which is determined from the reference profiles. The control force is acting for 200 sec and is determined by the previous PD control law after that. To produce constant control force with the increase of the relative distance between each drone craft and the sensor craft, the absolute values of the charges of drone craft slightly increases. This fact is shown between 750 sec and 950 sec in Figure 3.20. In Figure 3.22, each angular momentum

does not change due to the initial conditions and, in Figure 3.22, the final configuration is restricted to expand as far as possible.

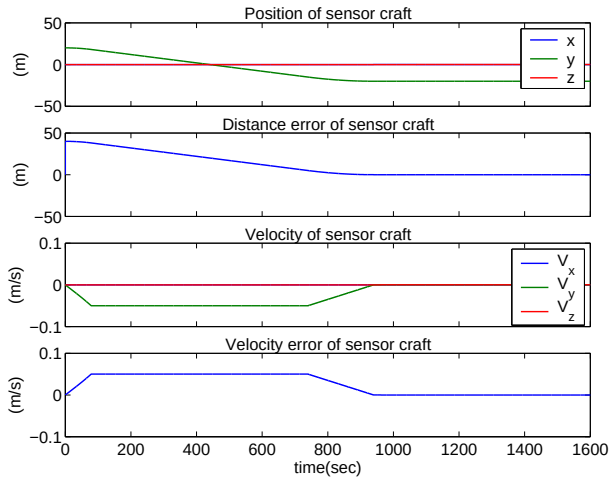

Figure 3.16: Case 5 - The velocity and position of sensor craft

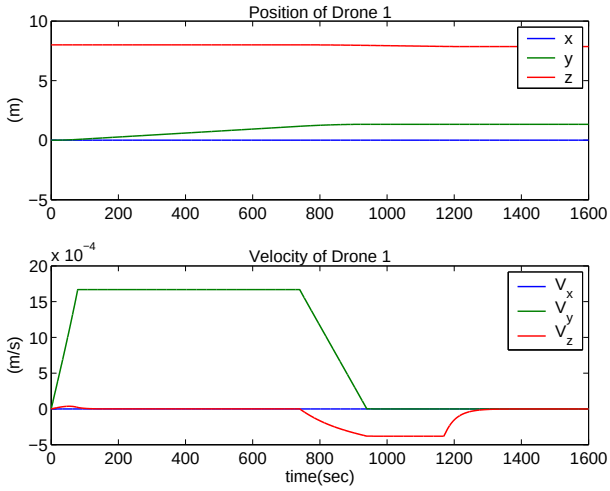

Figure 3.17: Case 5 - The velocity and position of 1st drone craft

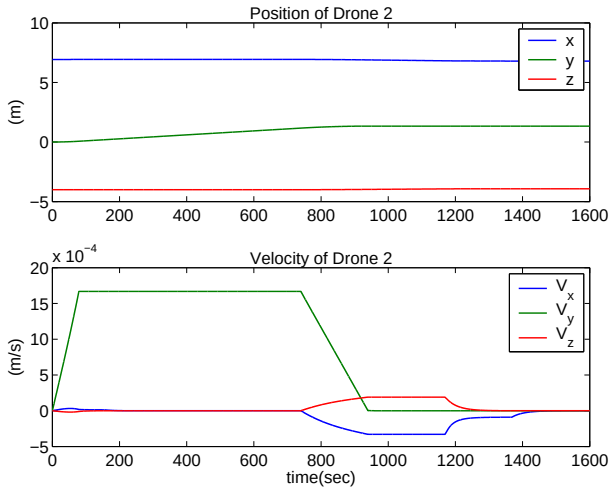

Figure 3.18: Case 5 - The velocity and position of 2nd drone craft

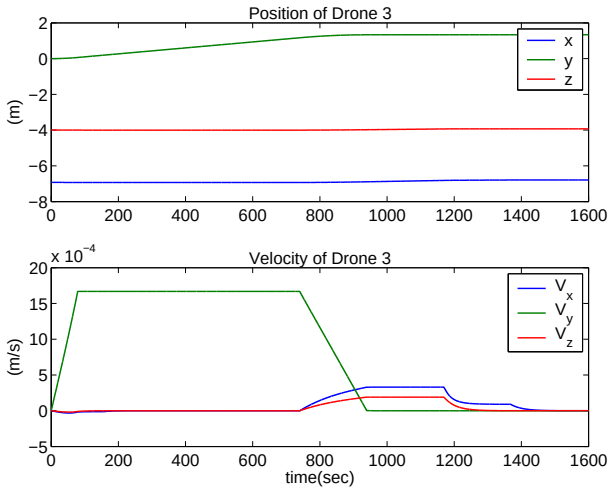

Figure 3.19: Case 5 - The velocity and position of 3rd drone craft

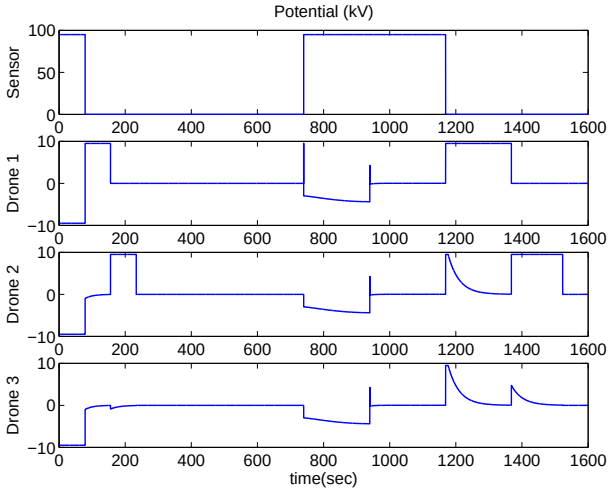

Figure 3.20: Case 5 - Charges

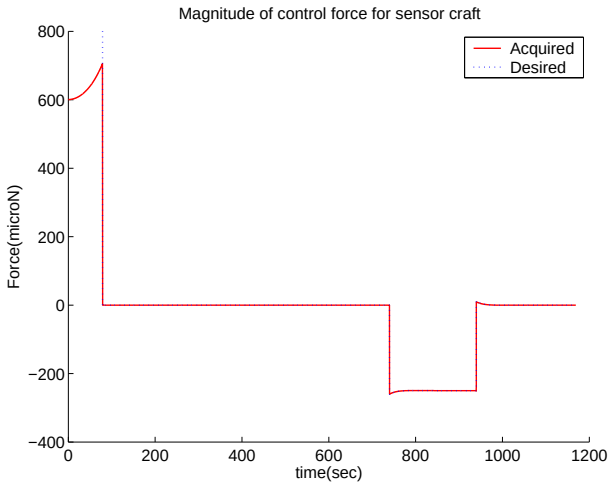

Figure 3.21: Case 5 - Coulomb control force

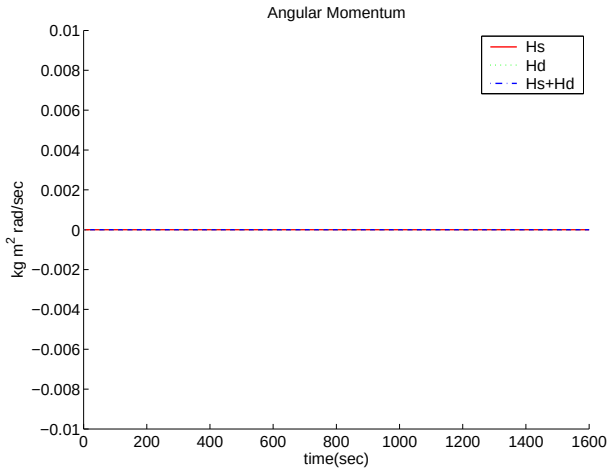

Figure 3.22: Case 5 - Angular momentum

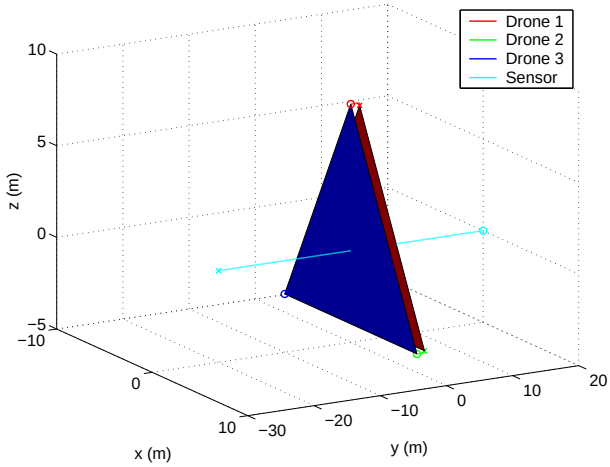

Figure 3.23: Case 5 - 3D locus

3.4.3 Coasting Line out of the Formation Center

In this simulation, the final position of the sensor craft is changed to (0, -20, 4) m. This means that the center of mass of the whole formation does not lie on the coasting line anymore. The initial and final conditions produce the rotation of the drone plane and this fact is already discussed in Section 3.2.

All spacecraft achieve the desired results as can be seen from Figures 3.24 through 3.27. When the sensor craft started to coast, all drone craft try to stop with the drone rest control. But it is impossible. Due to the rotation of the drone plane, the inertial y axis is not orthogonal to the drone plane anymore. The drone rest control during the coasting period tries to stop the drone craft on the drone plane, but it is impossible in this case. Figure 3.28 illustrates this statement clearly. During the coasting period, the first drone craft stops on the drone plane around 230 sec and the second and third drone craft try to stop after that. However, the rotating drone plane makes the first drone craft move away from the current stop position on the drone plane. The first drone shortly has nonzero velocity on the drone plane and the drone rest control works to stop the first drone craft. This control action is sustained until the sensor craft enters the deceleration band. The break response around 970 sec is due to the handover control method. As can be seen from Figure 3.29, the control forces look similar to the right plot of Figure 3.21, but the first part of the control force is smaller because the initial and final position of the sensor craft are different. In Figure 3.30, each angular momentum vector changes opposite direction, but after the sensor craft stops the angular momentum of the drone plane goes to zero. It is shown in Figure

3.31 that the final configuration of the drone craft does not expand heavily.

Several numerical simulations have been presented. They clearly show that the Bang-coast-bang control method has advantages against the bang-bang control method. Continuous control action may increase the possibility of control loss. The bang-coast-bang control method can lessen the worry about losing control and provide more predictable sensor placement control.

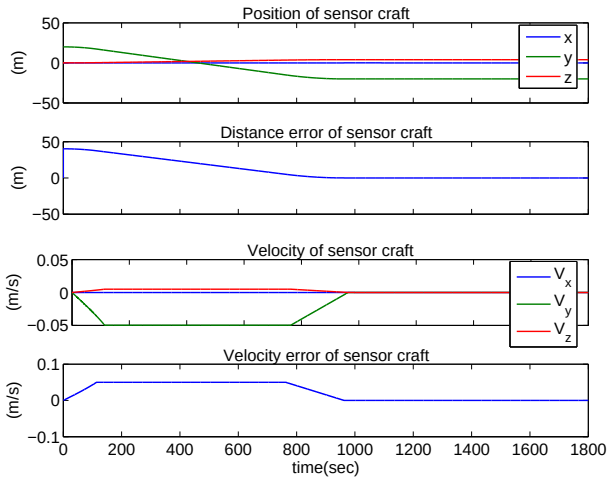

Figure 3.24: Case 6 - The velocity and position of sensor craft

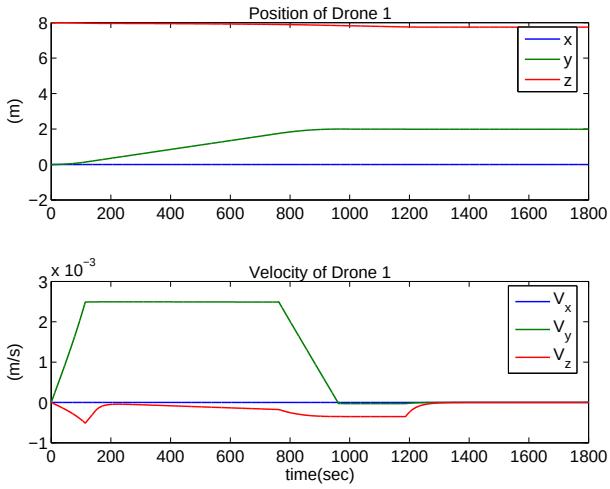

Figure 3.25: Case 6 - The velocity and position of 1st drone craft

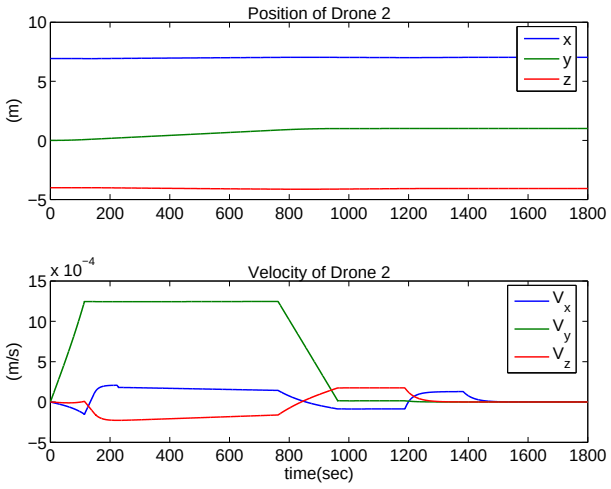

Figure 3.26: Case 6 - The velocity and position of 2nd drone craft

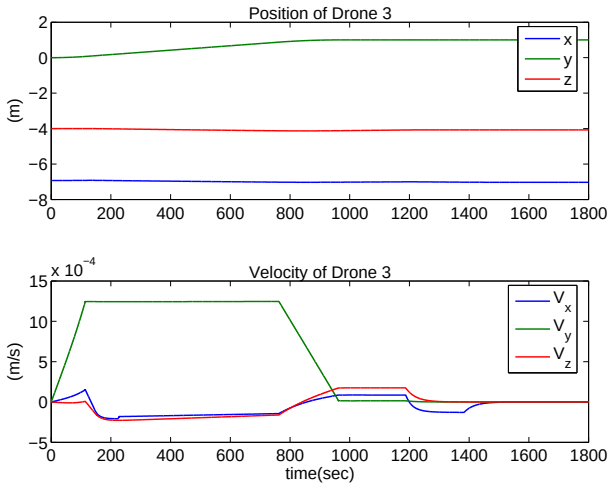

Figure 3.27: Case 6 - The velocity and position of 3rd drone craft

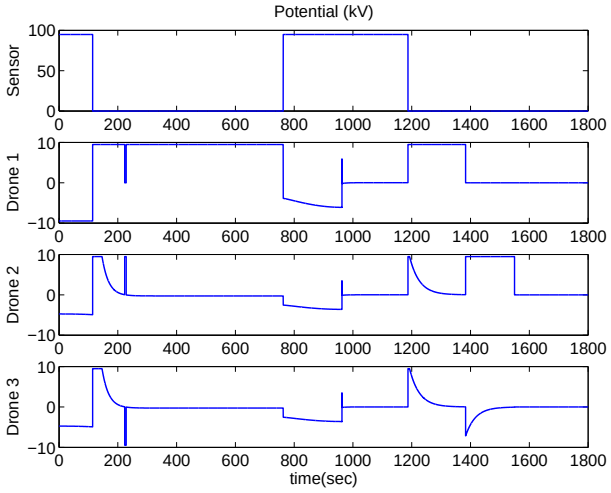

Figure 3.28: Case 6 - Charges

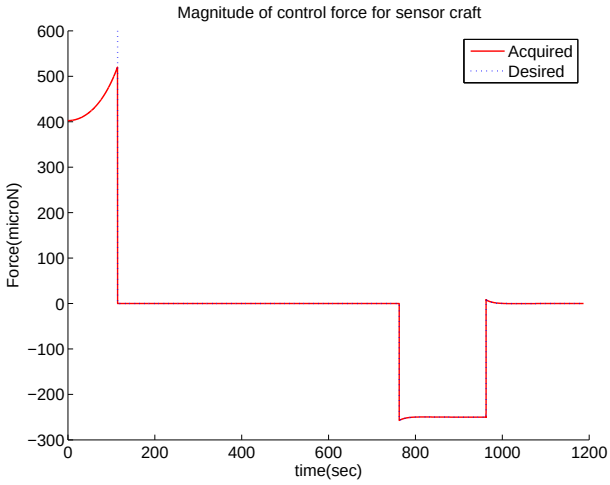

Figure 3.29: Case 6 - Coulomb control force

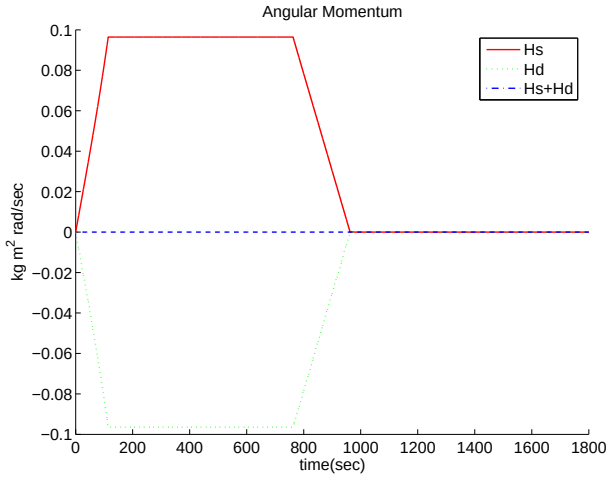

Figure 3.30: Case 6 - Angular momentum

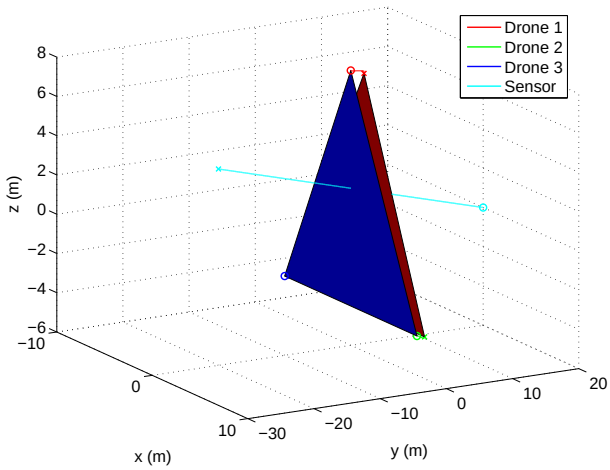

Figure 3.31: Case 6 - 3D locus

Chapter 4

Conclusion

A closely-flying formation for the space interferometry problem should avoid sensor contamination of thruster exhaust plumes. In a high Earth orbit, the Coulomb propulsion system has several strengths compared to conventional thruster systems. Because the Coulomb propulsion system produces essentially no physical flux, it has no effect on the sensors of neighboring spacecraft and there is essentially no propellant usage. These advantages are significant to space propulsion systems. However, this system is only applicable to a spacecraft formation in HEO or higher due to the characteristic of the space plasma environment. Coulomb forces are the internal forces of the formation and the change of the charge of one spacecraft affects the motion of all charged spacecraft. This fact makes the control development using Coulomb forces difficult. Thus, a sequential control method is proposed with consideration of the singularity of a drone plane in this study. During the first step, the sensor craft is controlled using the drone craft. After the sensor craft arrives at the final

position, the charge of the sensor craft is turned off. During the second step, the first drone craft velocity is canceled and then the second and third drone craft stop. It is assumed that all spacecraft are far from any planet, such that no orbital motion effects are included. The bang-bang control is used to the reposition control of a sensor craft considering the singularity of the drone plane. However, the bang-bang control may lose control of the formation as relative distances grow. To counter this weakness, a bang-coast-bang control method is proposed. Due to this control method, the flight time of a sensor craft can be adjusted by a coasting velocity and a deceleration force. In addition, system stability increases with the coasting period of a sensor craft.

Future research in this area may consider the following challenges. The drone rest control during a sensor craft coasting period is limited by the angular momentum change of the drone plane about the formation center. To solve this problem, a formation control method which has no limit of drone plane rotation should be developed, or a tether system can be adopted to maintain the drone craft formation. Formation shape control of the drone craft using only Coulomb forces is challenging. A tether formation system will help to reconfigure the drone formation, but will introduce large mechanical complexities. If the drone craft charges are turned on at a maximum value, then the drone craft will repel each other and the relative distances between the drone craft are limited by the tether length. In future work, the configuration of at least four drone craft will be considered to avoid the singularity of a drone plane. A tetrahedron formation of drone craft can produce a sensor control force in any direction. This method may help to solve the singularity problem with the redundant

drone craft. If the formation is to operate in high Earth orbit, then the orbital motion effect should be considered to increase the feasibility of this control system. The current research only studies inertial spacecraft motion, not orbital motion.

Bibliography

[1] Berryman, J. and Schaub, H., "Static Equilibrium Configurations in GEO Coulomb Spacecraft Formations," AAS Spaceflight Mechanics Meeting, Copper Mountain, Colorado, Jan. 23-27, 2005

[2] Chaisson, E.J., *The Hubble Wars : astrophysics meets astropholitics in the two-billion-dollar struggle over the Hubble Space Telescope*, HarperCollins Publishers, 1994

[3] Chong, J-H, *Dynamic Behavior of Spacecraft Formation Flying using Coulomb Forces*, Master's thesis, Michigan Technological University, Houghton, Michigan, May 2002

[4] Deshmukh, S.H., *Controlled Spacecraft Charging for Coulomb Force Control of Spacecraft Formations*, Master's thesis, Michigan Technological University, Houghton, Michigan, May 2002

[5] Elias, L.M., Kong, E.M., and Miller D.W., "An Investigation of Electromagnetic Control for Formation flight Applications," Proceedings of SPIE, 2002, Vol. 4849, pp.166-180

[6] Farley, R.E., and Quinn, D.A., "Tethered Formation Configurations: Meeting the Scientific

Objectives of Large Aperture and Interferometeric Scienc," AIAA Space Conference and Exposition, Albuquerque, NM, Aug.28-30, 2001

[7] Joe, H., Schaub, H., and Parker, G.G., "Formation Dynamics of Coulomb Satellites," 6th International Conference on Dynamics and Control of Systems and Structures in Space, Cinque Terre, Liguria, Italy, July 18-22, 2004.

[8] King, L.B., Parker, G.G., Deshmukh, S., and Chong, J-H, "Spacecraft Formation-flying using Inter-vehicle Coulomb Forces," Final report for Phase I research sponsored by NIAC-NASA Institute for Advanced Concepts, January 7, 2002

[9] Larson, W.J., and Wertz, J.R. (Editors), *Space Mission Analysis and Design*, 2nd Edition, Microcosm, Inc., and Kluwer Academic Publishers, 2001

[10] Mullen, E.G., Gussenhoven, M.S., and Hardy, D.A., "SCATHA Survey of High-Voltage Spacecraft Charging in Sunlight", *Journal of the Geophysical Sciences*, Vol. 91, 1986, pp. 1074-1090

[11] Natarajan, A. and Schaub, H., "Linear Dynamics and Stability Analysis of a Coulomb Tether Formation," AAS Spaceflight Mechanics Meeting, Copper Mountain, Colorado, Jan. 23-27, 2005

[12] Parker, G.G., Passerello, C.E., and Schaub, H., "Static Formation Control using Inter-spacecraft Coulomb Forces," 2nd International Symposium on Formation Flying Missions and Technologies, Washington, D.C., Sept. 14-16, 2004

[13] Schaub, H., Parker, G.G., and King, L.B., "Challenges and Prospects of Coulomb Spacecraft Formations," AAS John L. Junkins Symposium, College Station, Texas, May 22-23, 2003

[14] Schaub, H., and Junkins, J.L., *Analytical Mechanics of Space Systems*, AIAA Education Series, American Institute of Aeronautics and Astronautics, Inc., Reston, Virginia, 2003

[15] Schaub, H., "Stabilization of Satellite Motion Relative to a Coulomb Spacecraft Formation," AAS Spaceflight Mechanics Meeting, Maui, Hawaii, Feb. 8-12, 2004

[16] Schaub, H., and Kim, M., "Orbit Element Difference Constraints for Coulomb Satellite Formation," AAS Astrodynamics Specialists Conference, Providence, Rhode Island, Aug. 16-19, 2004

[17] Sengupta, P., and Vadali, S.R., "A Lyapunov-Based Controller for Satellite Formation Reconfiguration in the Presence of J_2 Perturbations," AAS/AIAA Space Flight Mechanics Meeting, Maui, Hawaii, February 8-12

[18] Sedwick, R.J., and Schweighart, S.A., "Propellantless spin-up of tethered or electromagnetically coupled sparse apertures," NASA Goddard Space Flight Center under SPECS, the NASA Institute for Advanced Concepts, 2003

[19] Torkar,K., Fehringer, M., Arends, H., Goldstein, R., Grard, R.J.L., Narheim, B.T., Olsen, R.C., Pedersen, A., Riedler, W., Rüdenauer, F., Schmidt, R., Svenes, K., Whipple, E., Torbert, R. and Zhao, H., "Spacecraft Potential Control Using Indium Ion Sources - Ex-

perience and Outlook Based on Six Years of Operation in Space," 6th Spacecraft Charging Technology Conference, September 2000, pp. 27-32

[20] Torkar, K., Riedler, W., Escoubet, C.P., Fehringer, M., Schmidt, R., Grard, R.J.L., Arends, H., Rüdenauer, F., Steiger, W., Narheim, B.T., Svenes, K., Torbert, R., André, M., Fazakerley, A., Goldstein, R., Olsen, R.C., Pedersen, A., Whipple, E., and Zhao, H., "Active Spacecraft Potential Control for Cluster - Implementation and First Results," *Annales Geophysicae*, 2001, pp. 1289-1302